from genetically engineered animals is still scarce, and *in vivo* validation of such findings is still much awaited. Furthermore, despite the heavy expression of all CaMKI isoforms in the developing forebrain, there is yet little information as to what kinds of endogenous activity or extracellular ligands may influence the activity of CaMKI, during a perinatal period when only spontaneous Ca^{2+} transients are generated, and when synaptic activity-driven Ca^{2+}-mobilization is still missing.

We previously reported that a dendritic raft-anchored CaMK, CaMKIγ/CL3, plays an essential role in dendritic growth downstream of BDNF (Takemoto-Kimura et al., 2007). However, the exact context in which other CaMKI isoforms might contribute to neuronal morphogenesis remained obscure.

Here, we show genetic and pharmacogenetic evidence that demonstrates that two separate limbs of CaMKK–CaMKI cascades, CaMKK–CaMKIα and CaMKK–CaMKIγ, critically coordinate axonal and dendritic morphogenesis of immature cortical neurons, respectively. Furthermore, we found that activation of $GABA_A$ receptors promoted axonal growth via the CaMKK–CaMKIα pathway. During perinatal brain development, *in vivo* knockdown of CaMKIα significantly impaired the terminal elongation of callosal axon projections in the somatosensory cortex. Together, our data suggest that a GABA-driven CaMK cascade may play a critical role in activity-regulated refinement of cortical axon wiring.

Materials and Methods

Construction of expression plasmids and RNA interference vectors. For RNA interference (RNAi) experiments, short hairpin RNA (shRNA) vectors, coexpressing mRFP1 as a morphological tracer, were constructed essentially as described previously (Takemoto-Kimura et al., 2007). To create pSUPER-shCaMKIα and pSUPER-shCaMKIα#2, two complementary 60 bp oligonucleotides carrying sense and antisense sequences for CATTGTAGCCCTGGATGAC (19 bp; corresponding to nucleotides 231-249 of mouse CaMKIα) and antisense and sense sequences for GATCAAGCACCCCAACATT (19 bp; corresponding to nucleotides 216-234 of mouse CaMKIα), respectively, were subcloned into the pSuper+mRFP1 plasmid backbone. pSUPER-shNega was generated similarly except that an artificial 19-mer sequence (ATCCGCGCGATAGTACGTA) was used as a target as described previously (Takemoto-Kimura et al., 2007). This sequence was based on a commercially available negative control small interfering RNA sequence (B-Bridge International), and we confirmed that it had no significant identity to any known mammalian gene based on a BLAST (basic local alignment search tool) search. Silent mutations were introduced into the shRNA target sequence of enhanced green fluorescent protein (EGFP)-tagged wild-type (WT) and mutant CaMKIα cDNAs to generate shRNA-resistant constructs (pEGFP-CaMKIα_{res} and related constructs). Short hairpin RNA interference vectors against CaMKIα, CaMKIγ/CL3, and CaMKIV [shCaMKIα (this study); shCaMKIγ/CL3 and shCaMKIV (Takemoto-Kimura et al., 2007)] selectively suppressed expression of GFP-CaMKIα, GFP-CaMKIγ/CL3, GFP-CaMKIV, respectively (supplemental Fig. 2*A*,*B*, available at www.jneurosci.org as supplemental material). An antibody against CaMKIV (BD Biosciences Transduction Laboratories) also confirmed these results. The potency of the knockdown was estimated to be ~70–80%, based on the reduction of overexpressed GFP-tagged proteins in Western blot analyses (supplemental Fig. 2*B*, available at www.jneurosci.org as supplemental material). In keeping with this, and consistent with a transfection efficiency of >50% in our electroporation, we also detected a target-specific decrease of 40~50% in the amount of endogenous mRNA using a real-time PCR system (LightCycler 1.5; Roche Diagnostics) (supplemental Fig. 2*C*, available at www.jneurosci.org as supplemental material).

Rat CaMKIα cDNA was inserted into pEGFPC1 vector (Clontech) to generate pEGFP-CaMKIα (Takemoto-Kimura et al., 2003). The expression vector for a constitutively active form, pEGFP-CaMKIαCA (286IHQS to 286EDDD; F307A) was created from pEGFP-CaMKIα by

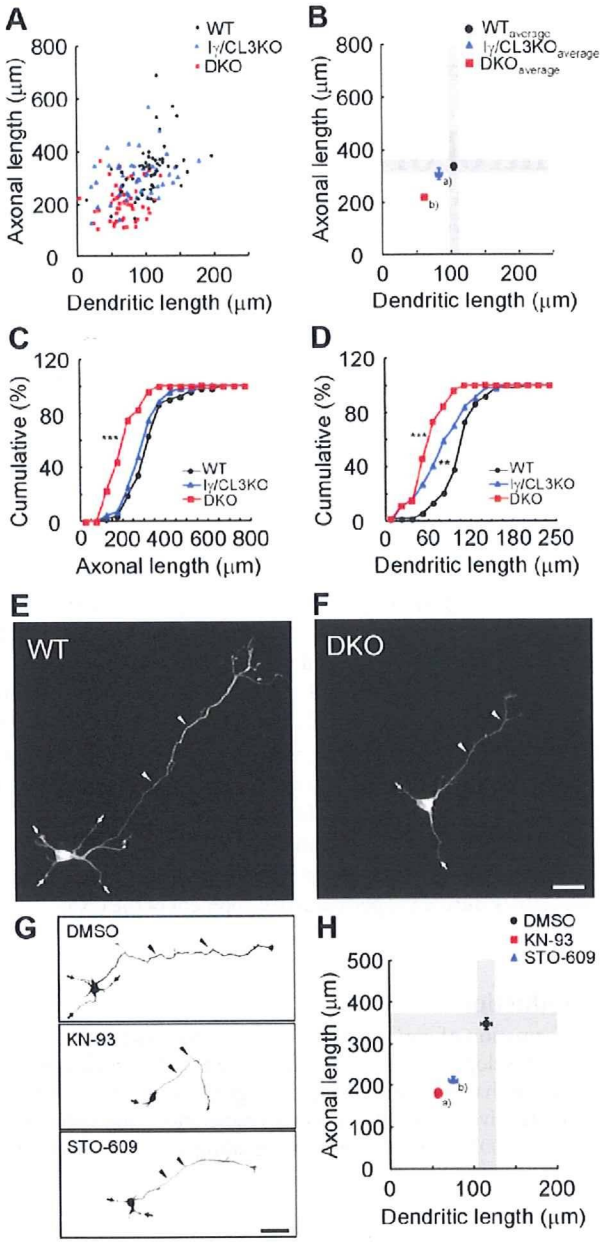

Figure 1. CaMKK-dependent CaMK cascades control cortical axonal and dendritic growth. ***A***, ***B***, A scattered plot (orthogonal plot) of data points (***A***) and averages (***B***) for both axonal and dendritic lengths obtained of individual neurons. Black circles, Wild type (WT). Blue triangles, Iγ/CL3 knock-out (Iγ/CL3 KO). Red squares, CaMKKα/β-double knock-out (DKO). Number of neurons: WT, $n = 52$; Iγ/CL3 KO, $n = 44$; DKO, $n = 52$. [a]Dendrite, $p < 0.01$; [b]Axon, $p < 0.001$; dendrite, $p < 0.001$ (one-way ANOVA with Tukey's test comparison with WT). ***C***, ***D***, Cumulative probability analysis for total axonal length (***C***) and total dendritic length (***D***) in neurons from WT, DKO, and Iγ/CL3 KO mice. Number of neurons: WT, $n = 52$; DKO, $n = 52$; Iγ/CL3 KO, $n = 44$. $^{**}p < 0.01$; $^{***}p < 0.001$, Kolmogorov–Smirnov test comparison with WT. ***E***, ***F***, Cortical neurons (2 d *in vitro*) from CaMKKα/β-DKO mice (***F***) showed impaired growth of axons (arrowheads) and dendrites (arrows) compared with neurons from WT mice (***E***). Scale bar, 25 μm. ***G***, Treatment with KN-93, a general CaMK inhibitor, and STO-609, a blocker of CaMKKα/β, the upstream kinases of all CaMKI/IV, from 6 to 48 h after plating impaired both axonal (arrowheads) and dendritic (arrows) growth. Scale bar, 50 μm. ***H***, An orthogonal plot shows a quantitative analysis of axonal and dendritic morphometric parameters from each neuron. Number of neurons: DMSO, $n = 48$; KN-93, $n = 43$; STO-609, $n = 48$. [a,b]Axon, $p < 0.001$; dendrite, $p < 0.001$ (one-way ANOVA with Tukey's test comparison with DMSO).

site-directed mutagenesis. Similarly, a point mutation was introduced to generate pEGFP-CaMKIαK49A. pCAG-EGFP-CaMKIγ/CL3 was as described previously (Takemoto-Kimura et al., 2007). CaMKKβ wild-type and V269F cDNA (Tokumitsu et al., 2003) (a kind gift from Dr. Hiroshi Tokumitsu, Kagawa University, Kagawa, Japan) was subcloned into pEGFPC3. Mouse CaMKIβ and CaMKIδ cDNAs were obtained from the German RZPD gene collection and RIKEN Genomic Science Center, respectively, and inserted into pEGFPC1 vector to generate pEGFP-CaMKIβ and pEGFP-CaMKIδ. All constructs were verified by sequencing.

Gene targeting, neuronal culture, and pharmacology. All animal experiments in this study were performed in accordance with regulations and guidelines for the care and use of the experimental animals of the University of Tokyo, and approved by the institutional review committee of University of Tokyo Graduate School of Medicine.

CaMKKα-knock-out (KO) mice were described previously (Blaeser et al., 2006). CaMKKβ-KO mice were produced similarly by deleting exon 2 (where the ATG starts) through exon 6 of the CaMKKβ gene. A detailed characterization of CaMKKβ-KO mice will be described elsewhere (F. Blaeser and T. A. Chatila, unpublished observations). CaMKKα- and CaMKKβ-KO mice were crossed to produce CaMKKα/β-double knock-out (DKO) mice. The targeting strategy of CaMKIγ/CL3-KO mice was as described previously (Takemoto-Kimura et al., 2007).

Dissociated cortical neurons were prepared and cultured from embryonic day 19 (E19) Sprague Dawley rats or E17 C57BL/6 mice (wild-type as well as mutant mice), essentially as described previously (Takemoto-Kimura et al., 2007). In brief, dissected cortices were incubated for 10 min with 10 mg/ml trypsin type XI (Sigma-Aldrich) plus 0.5 mg/ml DNase I type IV (Sigma-Aldrich) at room temperature and mechanically dissociated in Hanks solution, pH 7.4 (Sigma-Aldrich), with 0.5 mg/ml DNase I type IV and 12 mM $MgSO_4$. Cortical neurons were transfected immediately after dissociation by electroporation using a Nucleofector (Amaxa Biosystems), plated onto poly-L-lysine-coated 12 mm coverslips (BD Biosciences), poly-D-lysine-coated glass-bottom dishes (MatTek) or six-well dish (BD Biosciences), and maintained in minimum essential medium (Invitrogen) containing 5 g/L glucose, 0.2 g/L $NaHCO_3$, 0.1 g/L transferrin (Calbiochem), 2 mM GlutaMAX-I (Invitrogen), 25 μg/ml insulin (Sigma-Aldrich), B-27 supplement (Invitrogen), and 10% fetal bovine serum. Cultures were maintained in 5% CO_2 at 37°C.

For inhibition and stimulation experiments, 2-[*N*-(2-hydroxyethyl)-*N*-(4-methoxybenzenesulfonyl)] amino-*N*-(4-chlorocinnamyl)-*N*-methylbenzylamine (KN-93) (Calbiochem), 1,8-naphthoylene benzimidazole-3-carboxylic acid (STO-609) (Tocris Bioscience), mevastatin (Wako), muscimol (Tocris Bioscience), or BDNF [generously provided by Dainippon Sumitomo Pharma Co., Ltd. (Osaka, Japan) by courtesy of Dr. Chikao Nakayama] were added to the medium of cultured neurons expressing mRFP1 at 6 h after plating at the final concentrations of 10 μM (KN-93), 2.6 μM (STO-609), 10 μM (mevastatin), 1 μM (muscimol), and 50 ng/ml (BDNF), respectively. Bath application was performed by dissolving the reagents in one-half volume of the conditioned culture medium and by mixing this gently with the remaining one-half of the original medium in the dish. No medium change was done onward until fixation.

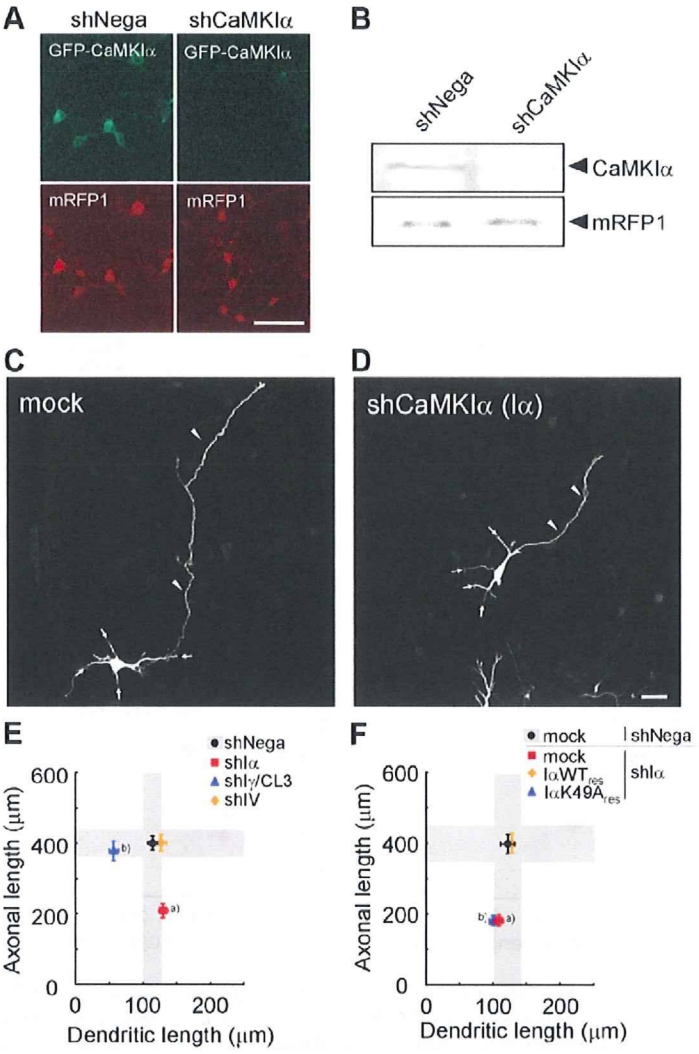

Figure 2. Knockdown of CaMKIα specifically impairs axonal but not dendritic growth. ***A***, Efficient downregulation of exogenous GFP-CaMKIα was achieved by a CaMKIα-targeted shRNA vector (shCaMKIα), but not by a control vector (shNega), in rat cortical neurons. The mRFP1 expression, which was driven by a dual promoter in a pSUPER+mRFP1 vector, remained unchanged. Scale bar, 50 μm. ***B***, Knockdown of endogenous CaMKIα was evaluated by Western blot analysis using an anti-CaMKIα antibody. Rat cortical neurons were transfected with pSUPER-shNega or pSUPER-shCaMKIα by electroporation, and the cells were lysed at 2 DIV. shCaMKIα suppressed endogenous CaMKIα, whereas the control mRFP1 expression level remained unchanged. ***C***, ***D***, shCaMKIα-expressing rat cortical neurons (shCaMKIα) (***D***) showed impaired axonal growth (arrowheads), whereas the dendritic morphology was spared (arrows) compared with neurons from shNega-expressing rat cortical neurons (shNega) (***C***). Scale bar, 25 μm. ***E***, An orthogonal plot of averaged data; $n = 15$ for all groups. [a]Axon, $p < 0.001$. [b]Dendrite, $p < 0.001$ (one-way ANOVA with Tukey's test comparison with shNega). Scale bar, 25 μm. ***F***, Introduction of shCaMKIα-resistant wild-type GFP-CaMKIα (WT_{res}) successfully rescued the axonal defect elicited by shCaMKIα. In contrast, an shCaMKIα-resistant kinase-inactive GFP-CaMKIα (a $K49A_{res}$ point mutant) was unable to rescue the shCaMKIα phenotype. $n = 15$ for all groups. [a,b]Axon, $p < 0.001$ (one-way ANOVA with Tukey's test comparison with shNega + mock).

Immunocytochemistry, morphometric analyses, and visualization of raft-targeted proteins. For morphometric analysis, cortical neurons were transfected immediately after dissociation by electroporation using Nucleofector and plated onto 12 mm poly-L-lysine-coated coverslips at the density of 5×10^5 cells (rats) or 7.5×10^5 cells (mice) per coverslip in 24-well plates. Dissociated cultures of rat and mouse cortical neurons and all measurements (axonal and dendritic length, axonal tip numbers) were performed at 2 d *in vitro* (DIV) essentially as described previously

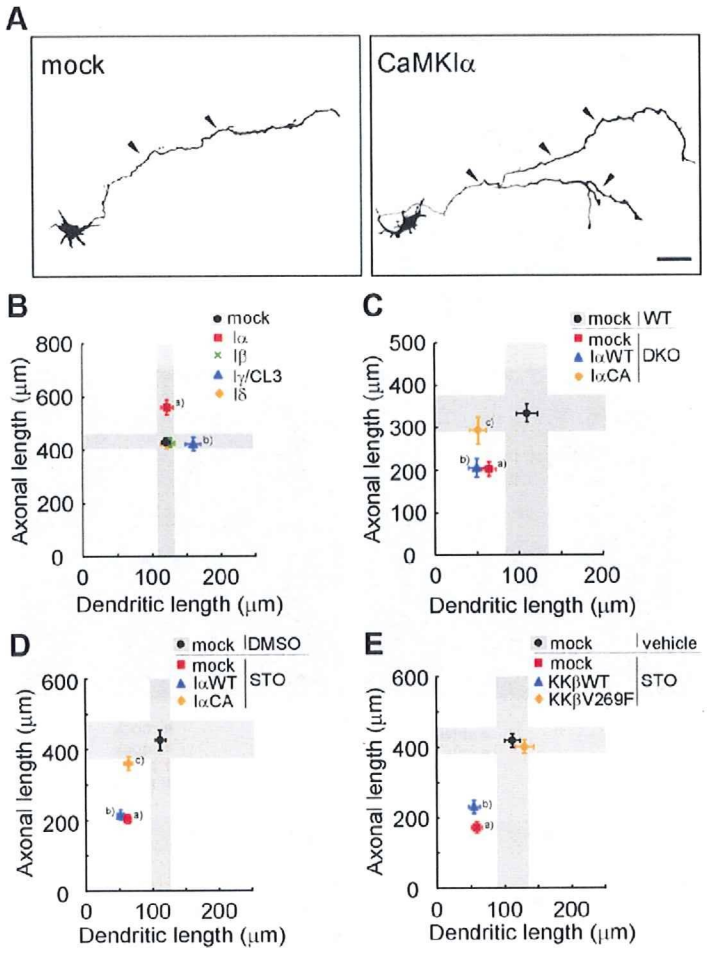

Figure 3. A specific role for a CaMKK–CaMKIα cascade in promoting axonal growth in cortical neurons. ***A***, Representative images of rat cortical neurons transfected with GFP-CaMKIα. Scale bar, 50 μm. ***B***, Overexpression of CaMKIα and CaMKIγ facilitated axonal and dendritic growth, respectively. $n = 15$ for all groups. [a]Axon, $p < 0.001$; [b]dendrite, $p < 0.05$ (one-way ANOVA with Tukey's test comparison with mock). ***C***, The axonal growth defect in DKO mice was selectively rescued by coexpression of a constitutively active CaMKIα (CaMKIαCA), but not by a wild-type CaMKIα (CaMKIαWT); the dendritic growth defect was left unaltered; $n = 15$ for all groups. [a]Axon, $p < 0.01$; dendrite, $p < 0.05$; [b]axon, $p < 0.01$; dendrite, $p < 0.001$; [c]dendrite, $p < 0.01$ (one-way ANOVA with Tukey's test comparison with WT plus mock). ***D***, Only the axonal growth defects caused by STO-609 treatment were rescued by expression of a constitutively active CaMKIα (CaMKIαCA), but not of a wild-type CaMKIα (CaMKIαWT). Dendritic growth defects remained unchanged; $n = 15$ for all groups. [a,b]Axon, $p < 0.001$; dendrite, $p < 0.001$; [c]Dendrite, $p < 0.001$ (one-way ANOVA with Tukey's test comparison with DMSO plus mock). ***E***, Both axonal and dendritic growth defects caused by STO-609 treatment were rescued by introducing an STO-609-resistant CaMKKβ mutant (V269F), but not a CaMKKβ-WT. n = 15 for all groups. [a,b]Axon, $p < 0.001$; dendrite, $p < 0.01$ (one-way ANOVA with Tukey's test comparison with vehicle plus mock).

(Takemoto-Kimura et al., 2007). Images of neuronal morphologies were captured based on immunoreactivities against GFP, mRFP1, or mCherry, using the Olympus BX51 microscopy system with a 20× objective. Dendrites and axons were identified by standard morphological criteria as described previously (Takemoto-Kimura et al., 2007), and only neurons that possessed one clearly classifiable axon and one or more dendrites were analyzed. All quantitative analyses were performed by an observer blinded to the identity of the transfected constructs, genotypes of mice, or treated drugs.

Immunostaining was performed as described previously (Bito et al., 1996; Nonaka et al., 2006; Takemoto-Kimura et al., 2007). A rabbit anti-DsRed antibody (Takara) was used for quantitative morphometric analyses of RNAi, rescue, and forced expression experiments, and a rat anti-GFP antibody (Nacalai Tesque) was used to detect coexpressed constructs. An anti-GM130 antibody (BD Biosciences Transduction Laboratories) was used as a Golgi marker. As secondary antibodies, Alexa 488-, Alexa 594-conjugated anti-mouse, anti-rabbit, and anti-rat IgG antibodies (Invitrogen) were used. Fluorescent images were taken by a confocal laser microscopy system (LSM 510META-V3.2; Carl Zeiss) built on an inverted microscope (Axiovert 200M; Carl Zeiss) with the 40× objective [Plan-Neofluar 40×/numerical aperture (NA) 1.3, oil; Carl Zeiss] or using a CCD camera-based imaging analysis system (an Olympus BX51 equipped with a DP-70 camera). Visualization of raft-targeted proteins was performed as described previously (Takemoto-Kimura et al., 2007).

Western blot analysis. For Western blot analysis, cortical neurons were transfected with pSUPER-shNega or pSUPER-shCaMKIα by electroporation using a Nucleofector and plated at a density of 5×10^6 cells in a six-well dish. At 2 DIV, the cells were lysed in lysis buffer containing 50 mM Tris-HCl, pH 6.8, 2% SDS, and 10% glycerol. A rabbit anti-CaMKIα antibody (Uezu et al., 2002) was used (a kind gift from Drs. Kohji Fukunaga and Jiro Kasahara, Tohoku University, Sendai, Japan). Chemiluminescence detection was performed using horseradish peroxidase-conjugated anti-rabbit IgG and ECL Plus reagent (GE Healthcare).

Calcium imaging. Fluorescent calcium imaging was performed essentially as described previously (Furuyashiki et al., 2002; Takemoto-Kimura et al., 2007). Twenty-four hours after plating, cortical neurons on glass-bottom dishes were loaded with Fluo-4 AM (2.5 μM; Dojindo Laboratories) for 30 min at room temperature. After wash, cells were incubated at 37°C in a stage CO_2 chamber (Tokai Hit Co., Ltd.) equipped on an LSM 510 META (Carl Zeiss). After baseline recording, a medium containing 20× muscimol (final concentration, 1 μM) was gently bath-applied. Fluorescence changes in the cell bodies of individual cells were analyzed using MetaMorph or ImageJ software, and data are expressed as $\Delta F/F_o$.

In utero *electroporation, data acquisition, and quantification of the terminal arborization of callosal axons. In utero* electroporation was performed as described previously (Mizuno et al., 2007). Equal amount of pSUPER-vectors (2 μg/μl) and pCAG-EGFP (2 μg/μl) were mixed together with the dye Fast Green (0.05%; Wako) for injection into the lateral ventricle. The postnatal brains [postnatal day 16 (P16)] were fixed by transcardial perfusion of 4% PFA in 0.1 M phosphate buffer followed by overnight immersive fixation in 4% PFA in PBS and then transferred to 30% sucrose in PBS for 1–2 d at 4°C. Serial coronal brain sections were prepared at 50 μm thickness by a cryostat (HM560; Microm), and every one section out of four was immunostained. Sections were permeabilized in 0.3% Triton X-100 in PBS, and then blocked in 5% normal goat serum, 1% BSA, and 0.3% Triton X-100 in PBS followed by fluorescent immunostaining of EGFP. Sections were counterstained with DAPI (4′,6′-diamidino-2-phenylindole) (Invitrogen). Quantitative analyses were performed and compared using the utmost posterior section of the stained sets that included the corpus callosum.

Confocal images were taken (LSM 510META-V3.2; Carl Zeiss) with a 10× objective (Plan-Neofluar 10×/NA 0.3; air; Carl Zeiss) with 10 μm optical sectioning. *Z* projection images taken at 512 × 512 pixels were acquired by average projection mode and background was subtracted, and the intensity was normalized by maximal intensity in the white mat-

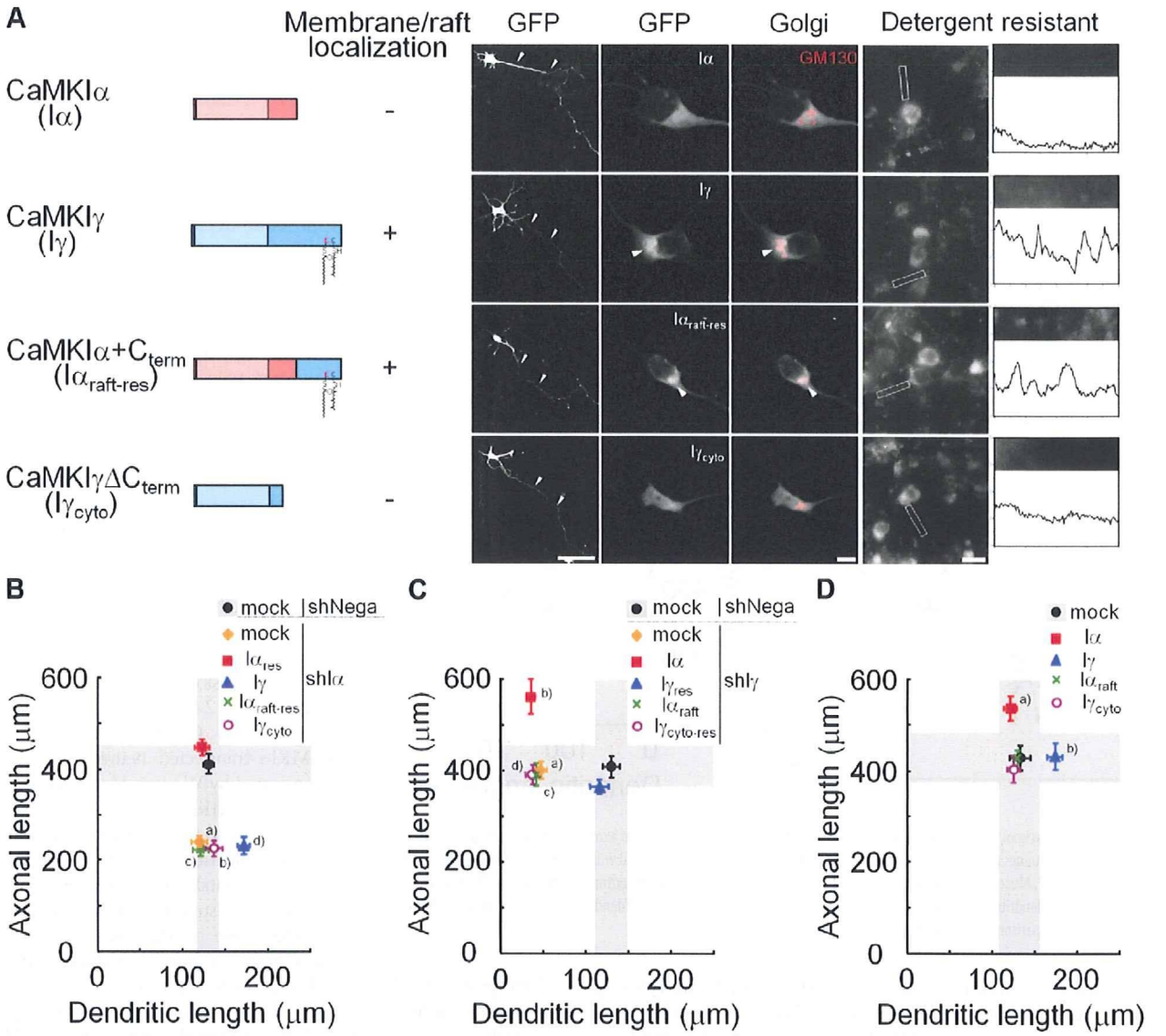

Figure 4. Functional segregation of CaMKK–CaMKIα and CaMKK–CaMKIγ cascades. ***A***, The domain structures and subcellular localizations of CaMKIα (Iα), CaMKIγ/CL3 (Iγ), and their chimeras. GFP-CaMKIα (Iα), CaMKIγ/CL3 (Iγ), and their chimeras distribution detected by anti-GFP immunostaining showed colocalization with a Golgi marker, GM130. GFP-Iγ and $Iα_{raft-res}$ signals were also enriched within Golgi (arrowheads). Single representative confocal sections are shown for Golgi localization. GFP-Iγ and -$Iα_{raft-res}$ fluorescence was retained after detergent treatment in a punctate manner in 2 DIV cortical neurons along the dendrites, demonstrating a sizable portion of detergent-resistant GFP-Iγ and $Iα_{raft-res}$ in the dendritic rafts. Line scans of pixel fluorescence, performed within a chosen field of a 15 μm dendritic segment. Scale bars: right, 50 μm; middle, 5 μm; left, 100 μm. ***B***, Neither Iγ, $Iα_{raft-res}$, nor $Iγ_{cyto}$ were able to rescue the axonal phenotype caused by knockdown of CaMKIα; $n = 15$ for all groups. ^{a,b,c}Axon, $p < 0.001$; ^{d}axon, $p < 0.001$, dendrite, $p < 0.01$ (one-way ANOVA with Tukey's test comparison with shNega plus mock). ***C***, Neither Iα, $Iα_{raft}$, nor $Iγ_{cyto-res}$ were able to rescue the dendritic phenotype caused by knockdown of CaMKIγ/CL3; $n = 15$ for all groups. ^{a,c,d}Dendrite, $p < 0.001$; ^{b}axon, $p < 0.001$, dendrite, $p < 0.001$ (one-way ANOVA with Tukey's test comparison with shNega plus mock). ***D***, Overexpression of CaMKIα, specifically increased axon length in cortical neurons; $n = 15$ for all groups; $n = 15$ for all groups. ^{a}Axon, $p < 0.05$; ^{b}dendrite, $p < 0.001$ (one-way ANOVA with Tukey's test comparison with mock).

ter. For one-dimensional fluorescence intensity profile analysis in Figure 7*C*, a rectangular zone (nominal width set at 100 pixels) was drawn along the vertical axis from the pial surface to the white matter, and the average pixel intensity projected onto the vertical axis was calculated. To quantify the impairment of the cortical wiring in Figure 7*D*, average intensity in a rectangle region (100 pixels in width) in the cortex was divided by that in the white matter. Three to five pups were used for quantification. All calculations were performed using MetaMorph software (version 7; Molecular Devices).

Statistical analyses. Statistical analyses were run separately for axonal and dendritic datasets throughout our study, while using scattered diagrams of paired data of axonal and dendritic lengths ("orthogonal plots"). Statistical analyses were performed using Prism 4.0 (GraphPad Software). Student's *t* test was used for comparisons of two groups. One- or two-way ANOVA with *post hoc* Tukey–Kramer or Bonferroni's test was used for factorial analysis among more than three groups. Kolmogorov–Smirnov test was applied to Figure 1, *C* and *D*. All data are shown as mean ± SEM, unless otherwise mentioned, and shaded regions in orthogonal plots graphically depict the zone of mean ± 2SEM on both axes to facilitate the evaluation of the phenotypes.

Results

CaMKK pathway regulates axonal and dendritic growth during early stages of cortical development

We previously reported that a dendritic raft-anchored CaMKIγ/CL3 (Takemoto-Kimura et al., 2003) plays an essential role in

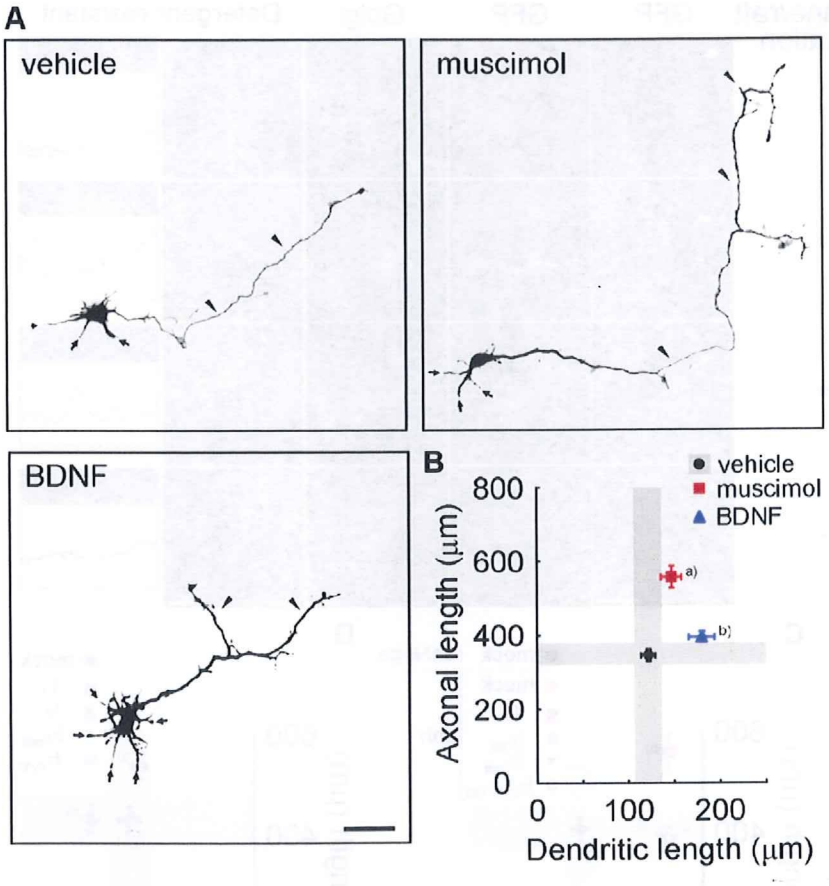

Figure 5. Muscimol, a $GABA_A$ receptor agonist, specifically stimulates elongation of axons in cultured cortical neurons. ***A***, ***B***, Representative images (***A***) and ensemble data (***B***) of immature cortical neurons treated with either muscimol (a $GABA_A$ receptor agonist) or BDNF. Muscimol significantly promoted axonal growth (arrowheads). In contrast, BDNF had no effect on axons but mainly affected dendrites. Scale bar, 50 μm. $n = 15$ for all groups. [a]Axon, $p < 0.001$; [b]dendrite, $p < 0.01$ (one-way ANOVA with Tukey's test comparison with vehicle).

dendritic growth downstream of BDNF during the morphological maturation of cortical neurons (Takemoto-Kimura et al., 2007). As four distinct CaMKI isoforms (α, β, γ/CL3, and δ) and CaMKIV are activated by upstream CaMKKs α and β, we sought to test how potently neuritogenesis was disturbed in cultured cortical neurons generated from CaMKKα/β-DKO mice. To specifically identify the genotype contribution to either axonal or dendritic growth, we orthogonally plotted the dendritic length (i.e., total length of all dendritic processes) and axonal length (i.e., total length of all axonal processes including branches) for each GFP-expressing cortical neuron blindly chosen from multiple fields of view (Fig. 1*A*,*B*; supplemental Fig. 1, available at www.jneurosci.org as supplemental material). Although cortical neurons from CaMKIγ/CL3 knock-out mice revealed a strikingly dendrite-specific deficit (Fig. 1*A–D*), we found that both axons and dendrites were significantly shortened in cortical neurons from DKO mice, compared with neurons from WT mice (Fig. 1*A–F*). Exposure to KN-93, which blocks all CaMK species (CaMKII, CaMKI, CaMKIV, and CaMKK), also reduced both total axonal and dendritic lengths (Fig. 1*G*,*H*). Specific blockade of the CaMKKs, using STO-609, a selective inhibitor for CaMKKs (Tokumitsu et al., 2002), resulted in a quantitatively similar impairment (Fig. 1*G*,*H*). Together, these genetic and pharmacological experiments clearly demonstrated that CaMKK-mediated CaMK cascades played critical roles both in axonogenesis and dendritogenesis of immature cortical neurons, consistent with a previous work on other cell types (Wayman et al., 2004). Furthermore, our data pointed to the presence of a selective CaMKK–CaMK cascade that strongly supported cortical axonal growth in a manner that was distinct from the dendritic contribution of CaMKIγ.

Suppression of CaMKIα expression specifically impairs axonal but not dendritic growth

To identify which of CaMKI or CaMKIV isoform(s) was involved in regulation of the axonal growth, we designed several short hairpin-type pSUPER vectors that were targeted to specific isoforms of the CaMKI/IV subfamily members. In this RNAi experiment, we also coexpressed a PGK promoter-driven mRFP1 as a morphological tracer. In a control experiment, polarized cortical neurons grown for 48 h typically grew 5~6 dendrites and a single axon. Knockdown using an shCaMKIα vector was prominent enough such that even an overexpressed GFP-CaMKIα became barely detectable 48 h after transfection, whereas the control mRFP1 expression level remained unchanged (Fig. 2*A*). Strong suppression of endogenous CaMKIα expression in shCaMKIα-transfected neurons was also demonstrated by Western blot analysis using an anti-CaMKIα antibody (Fig. 2*B*). A lack of cross-knockdown effects across α-, γ-CaMKI isoforms and CaMKIV was verified (supplemental Fig. 2, available at www.jneurosci.org as supplemental material).

Under these conditions, shCaMKIα-treated neurons showed unchanged dendritic growth but had a markedly shorter axon (Fig. 2*C*,*D*). Under the same conditions, in contrast, CaMKIγ/CL3 knockdown specifically blocked dendritic, but not axonal, outgrowth (Fig. 2*E*) (Takemoto-Kimura et al., 2007), whereas CaMKIV knockdown had no effect (Fig. 2*E*). The striking specificity in the axonal phenotype of CaMKIα was replicated even when axonal growth was measured under conditions in which shCaMKIα-transfected neurons were kept in suspension culture for an extended period (48 h) before plating, to ensure a maximized knockdown efficiency (supplemental Fig. 3, available at www.jneurosci.org as supplemental material). The impairment in axonal growth observed in CaMKIα-diminished neurons was rescued by expression of an shCaMKIα-resistant WT-CaMKIα (WT_{res}), but not by that of an shCaMKIα-resistant kinase-inactive CaMKIα ($K49A_{res}$), demonstrating the requirement of the kinase activity of CaMKIα (Fig. 2*F*). Together, our results strongly implicated the CaMKK–CaMKIα cascade as a critical player in the control of cortical axonal growth.

Two separate CaMKK–CaMKI cascades control cortical axonal and dendritic growth

In keeping with this robust selectivity in the knockdown experiments, forced expression of either one of the four CaMKI isoforms revealed that total axonal length was stimulated only by an

increase in CaMKIα, whereas dendrite growth was promoted only by CaMKIγ/CL3 expression (Fig. 3*A*,*B*). No change in primary axon number was detected in CaMKIα-overexpressing neurons, suggesting that CaMKIα did not act on axon specification per se (data not shown). Most critically, expression of a constitutively active CaMKIα (CaMKIαCA), was sufficient to rescue the axonal deficit, but without altering dendritic atrophy, in cortical neurons from DKO mice (Fig. 3*C*) or in WT neurons treated with STO-609 (Fig. 3*D*). However, forced expression of CaMKIαWT, which enzymatically remains inactive in the absence of CaMKK activity, had no effect in either of these backgrounds (Fig. 3*C*,*D*). In a parallel experiment, both axonal and dendritic defects in WT neurons treated with STO-609 were rescued by transfection of a STO-609-resistant CaMKKβ V269F mutant (Tokumitsu et al., 2003) (Fig. 3*E*).

Together, these data strongly implicated the CaMKK–CaMKIα and CaMKK–CaMKIγ cascades as parallel pathways acting independently in the promotion of axonal and dendrite growth, respectively, in cultured cortical neurons.

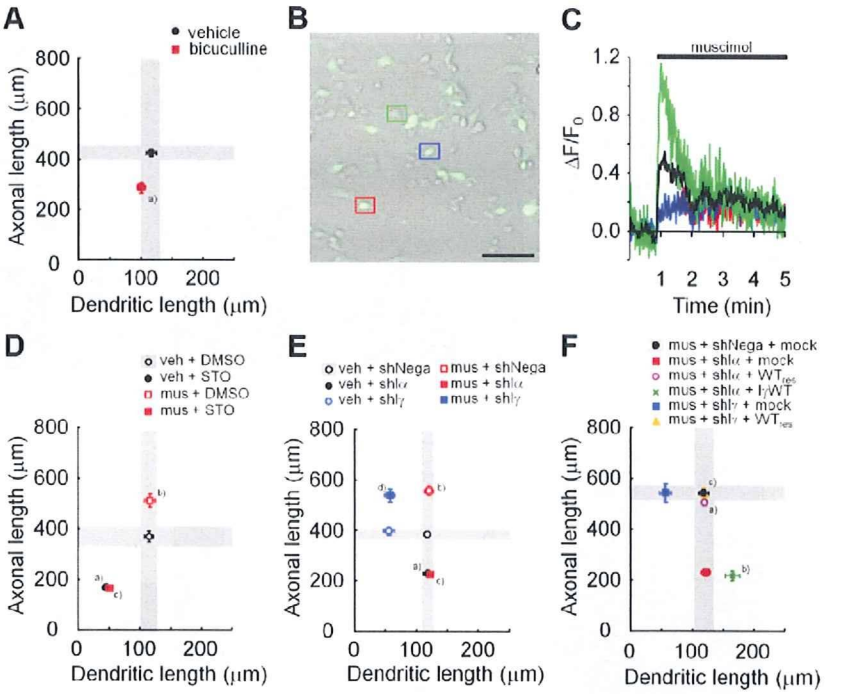

Figure 6. Activation of $GABA_A$ receptors promotes axonal growth via the CaMKK–CaMKIα pathway in immature cortical neurons. ***A***, Bicuculline, a $GABA_A$ receptor antagonist, blocked axonal growth; $n = 15$ for all groups. [a]Axon, $p < 0.001$ (Student's *t* test comparison with vehicle). ***B***, Embryonic cortical neurons (1 DIV) were loaded with a calcium indicator, Fluo-4 AM, and calcium responses were measured by time-lapse imaging. A green fluorescence image was overlaid on a differential interference contrast image. The colored boxes indicate the location of cells shown in ***C***. Scale bar, 50 μm. ***C***, Representative calcium responses in individual cells after muscimol administration. Three different types of calcium responses were revealed (green, blue, and red). An averaged response from 10 cells in a microscopic field is revealed in black. ***D***, Both basal and muscimol-stimulated axonal growths were suppressed with STO-609, a specific blocker of CaMKKα/β; $n = 15$ for all groups. Axon: two-way ANOVA, muscimol effect, $F_{(1,56)} = 14.38, p = 0.0004$; drug effect, $F_{(1,56)} = 225.63, p < 0.0001$; muscimol × drug, $F_{(1,56)} = 15.79, p = 0.0002$. Dendrite: two-way ANOVA, muscimol effect, $F_{(1,56)} = 0.39$, $p = 0.5336$; drug effect, $F_{(1,56)} = 105.76$, $p < 0.0001$; muscimol × drug, $F_{(1,56)} = 0.13, p = 0.7199$. [a,b]Axon, $p < 0.001$ (comparison with vehicle plus DMSO); [c]axon, $p < 0.001$ (comparison with muscimol plus DMSO); n.s. (comparison with vehicle plus STO). ***E***, CaMKIα knockdown quantitatively inhibited axonal growth induced by muscimol treatment, to an extent similar to that obtained with STO-609; $n = 15$ for all groups. Axon: two-way ANOVA, muscimol effect, $F_{(1,84)} = 66.44, p < 0.0001$; RNAi effect, $F_{(2,84)} = 168.04, p < 0.0001$; muscimol × RNAi, $F_{(2,84)} = 19.96, p < 0.0001$. Dendrite: two-way ANOVA, muscimol effect, $F_{(1,84)} = 0.23, p = 0.6305$; RNAi effect, $F_{(2,84)} = 61.58$, $p < 0.0001$; muscimol × RNAi, $F_{(2,84)} = 0.01$, $p = 0.9888$. [a,b]Axon, $p < 0.001$ (comparison with vehicle plus shNega); [c]axon, $p < 0.001$ (comparison with muscimol plus shNega); n.s. (comparison with vehicle plus shIα); [d]axon, $p < 0.001$ (comparison with vehicle plus shIγ); n.s. (comparison with muscimol plus shNega). ***F***, Introduction of shCaMKIα-resistant wild-type GFP-CaMKIα (WT_{res}) specifically rescued the suppression of muscimol-induced axonal growth triggered by knockdown of CaMKIα; $n = 15$ for all groups. [a]Axon, $p < 0.001$; dendrite, n.s.; [b]axon, n.s.; dendrite, $p < 0.001$ (one-way ANOVA with Tukey's test comparison with muscimol plus shIα plus mock); [c]axon, n.s.; dendrite, $p < 0.001$ (*t* test comparison with muscimol plus shIγ plus mock).

Both localization and kinase specificity of CaMKIα play important roles in CaMKIα-dependent axonal growth

Our data, so far, suggested that the axonogenic action of CaMKIα manifested in a manner that was completely orthogonal and independent to the dendritogenic effect mediated by CaMKIγ/CL3, despite a high degree of structural identity (71% amino acid identity in the catalytic domain sequences). What then discriminated the distinct function of these two kinases?

To identify the molecular determinants involved in axonogenic and dendritogenic selectivity of the CaMKK–CaMKI cascades, we generated CaMKIα/γ chimeras such that each kinase domain was paired with either cytosolic or Golgi/raft localization signals in the C terminus (Fig. 4*A*) (Takemoto-Kimura et al., 2007). We then tested their potencies to rescue the defect caused by knockdown of endogenous CaMKIα. As expected, forced expression of an shCaMKIα-resistant WT-CaMKIα ($I\alpha_{res}$) rescued the axonal impairment in CaMKIα knockdown neurons (Fig. 4*B*). The WT-CaMKIγ/CL3 (Iγ), however, promoted dendritic growth without showing any effect on axonal deficit. CaMKIα is believed to be freely diffusible. However, the C-terminal region of CaMKIγ/CL3 is lipidified by prenylation and palmitoylation, targeting it preferentially into lipid rafts, which are highly abundant in dendrites and in Golgi (Takemoto-Kimura et al., 2007) (Fig. 4*A*; supplemental Fig. 4, available at www.jneurosci.org as supplemental material). A dendritic raft-targeted mutant of CaMKIα, GFP-CaMKIα+C_{term} ($I\alpha_{raft\text{-}res}$), was unable to rescue the axonal impairment in CaMKIα knockdown neurons (Fig. 4*B*). A cytoplasmic, raft-excluded mutant of CaMKIγ/CL3, namely CaMKIγ/ CL3ΔC_{term} ($I\gamma_{cyto}$), had no ability, either (Fig. 4*B*), contrary to our expectations. Thus, surprisingly, CaMKI-mediated selectivity of neurite growth might not be simply determined by the localization of a CaMKIα or CaMKIγ in or out of the membrane rafts.

To further confirm this, the chimeras were expressed in the background of CaMKIγ/CL3-knockdown neurons. Expression of an RNAi-resistant WT-CaMKIγ/CL3 ($I\gamma_{res}$) rescued the dendritic impairment, whereas WT-CaMKIα (Iα) promoted axonal growth without an effect on dendrite impairment (Fig. 4*C*). Again, however, neither a freely diffusible CaMKIγ/CL3ΔC_{term} ($I\gamma_{cyto\text{-}res}$), nor a raft-targeted CaMKIα, CaMKIα+C_{term} ($I\alpha_{raft}$), had any effect (Fig. 4*C*). Furthermore, forced expression of CaMKIα, CaMKIγ, and CaMKIα/γ chimeras in a naive background revealed that total axonal length was stimulated only by

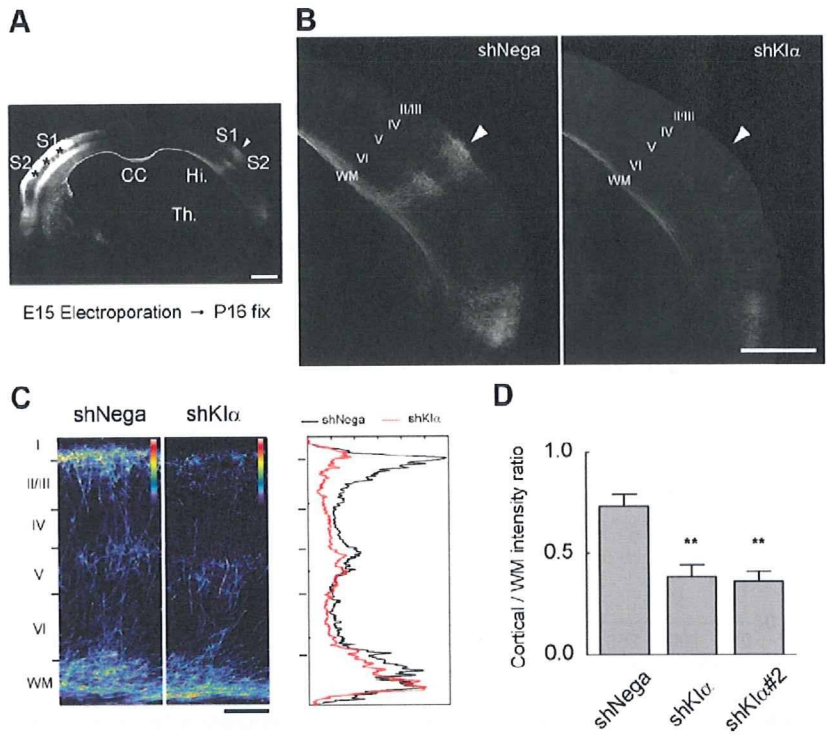

Figure 7. Knockdown of CaMKIα impairs terminal extension of callosal axons *in vivo*. ***A***, A control coronal section was obtained near the posterior end of the corpus callosum, from a P16 pup electroporated *in utero* with pSUPER-shNega and pCAG-EGFP on E15.5. The somatodendritic regions of layer II/III neurons were strongly labeled (asterisks) in the somatosensory cortex, from which callosal axons projected toward the contralateral cortical areas at the S1/S2 border region (arrowhead). Scale bar, 1 mm. CC, Corpus callosum; Hi, hippocampus; Th, thalamus. ***B***, Terminal extension of callosal axons into the contralateral cortical layers was severely disrupted in CaMKIα-knockdown neurons (shKIα), although axons were able to reach the white matter (WM) beneath S1/S2 area (arrowhead). Scale bar, 1 mm. ***C***, Axonal extension and terminal branch arborization were strongly impaired in layers II/III in CaMKIα-knockdown neurons, as illustrated by the magnified images of GFP marker showing the total axonal volumes present in the cortical layers (in pseudocolor), or by a one-dimensional fluorescence intensity profile analysis. Scale bar, 200 μm. ***D***, Quantification of the cortical wiring defect caused by an aberrant terminal axon extension in the cortex. Two independent RNAi constructs (shKIα and shKIα #2) gave similar results. $^{**}p < 0.01$ (one-way ANOVA with Tukey's test comparison with shNega).

an increase in CaMKIα (Fig. 4*D*). Together, these data provide strong functional evidence in support of the notion that CaMKK–CaMKIα and CaMKK–CaMKIγ are not duplicative mechanisms with simply altered targeting of downstream kinases, but are genuinely segregated cascades that are divergent at the level of kinase substrate specificity.

GABA is one of the physiological ligand acting upstream of CaMKIα to promote axonal growth during early stages of cortical development

The biological significance of this specificity could be demonstrated if the physiological signal triggering the axonogenic effect of CaMKIα was identified. To this end, we searched for a potential extracellular ligand that induced intracellular calcium elevation and potently stimulated axonal growth. We found that muscimol, a $GABA_A$ receptor agonist with a known excitatory action during perinatal development (Owens et al., 1996; Represa and Ben-Ari, 2005), specifically promoted elongation of axons, but not of dendrites, in cultured cortical neurons (Fig. 5*A*,*B*). Under the same conditions, we confirmed that BDNF had a complementary growth effect mostly selective for dendrites (Takemoto- Kimura et al., 2007).

To test the extent of requirement for GABA, we added bicuculline, a $GABA_A$ receptor antagonist, in the medium and found that axonal growth was rather selectively impaired (Fig. 6*A*). Furthermore, we confirmed that muscimol application triggered a strong Ca^{2+} influx in our cortical neurons (Fig. 6*B*,*C*). In keeping with this, forced expression of KCC2, a neuronal K^+/Cl^- cotransporter that lowers intracellular Cl^- concentration, and that is upregulated during development to convert the GABA action from excitation to inhibition (Rivera et al., 1999), impaired both constitutive and muscimol-stimulated axonal growth (supplemental Fig. 5, available at www.jneurosci.org as supplemental material). Pharmacological blockade of all CaM kinases using KN-93 (supplemental Fig. 6, available at www.jneurosci.org as supplemental material), or of CaMKK using STO-609 (Fig. 6*D*), completely blocked the axonogenic muscimol effect. CaMKIα RNAi (shIα), but not CaMKIγ/CL3 RNAi (shIγ), selectively impaired muscimol-stimulated axonal growth (Fig. 6*E*), and this effect was rescued by coexpressing an shCaMKIα-resistant CaMKIα WT ($I\alpha WT_{res}$), but not CaMKIγ/CL3 WT (IγWT) (Fig. 6*F*). Thus, a CaMKK–CaMKIα cascade may critically mediate $GABA_A$-stimulated axon outgrowth during the early development of a cortical neuron.

Contribution of CaMKIα in fine-tuning axonal pathfinding *in vivo*

We finally tested the *in vivo* relevance of these findings by investigating the function of CaMKIα during activity-dependent cortical wiring *in vivo*. The callosal axons that originate from layer II/III pyramidal neurons of the somatosensory cortex are known to elongate and target themselves to the border between the S1 and S2 areas of the contralateral cortex, where they suddenly turn and grow into the cortical layers and develop their terminal branches mainly at layers II–III and V. Previous reports demonstrated that reduction of neuronal excitability by overexpression of an inwardly rectifying potassium channel, Kir2.1, impaired such layer-specific development of the terminal branches in the visual cortex (Mizuno et al., 2007) and in the somatosensory cortex (Wang et al., 2007). Furthermore, premature elimination of excitatory GABA drive by forced expression of KCC2 or knockdown of NKCC1 in newly born cortical neurons dramatically perturbed the morphological maturation of the dendrites (Cancedda et al., 2007; Wang and Kriegstein, 2008) or of the terminal callosal axon branches (H. Mizuno, T. Hirano, and Y. Tagawa, unpublished data).

If the morphogenetic effect of excitatory GABA required Ca^{2+} signaling, could the CaMKK–CaMKIα pathway perhaps mediate activity-dependent control of callosal axonal extension? To test this, CaMKIα was knocked down in the somatosensory layer II/III neurons by *in utero* electroporation at E15.5, and an effect on axonal growth was examined. At P16, control neurons terminated their axons into a restricted region (border of S1/S2 area) in the contralateral cortex and extensively developed their terminal

branches into layers II/III and V (Fig. 7*A*). CaMKIα-knockdown neurons extended interhemispheric axonal projections in the white matter, suggesting the CaMKIα may not be absolutely required for midline crossing and progression of axon fibers (Fig. 7*B*). However, their terminal axonal extension into the cortical layers was severely diminished, especially in layers II/III (Fig. 7*C*,*D*). These results indicate a developmentally critical role of CaMKIα in activity-dependent regulation of cortical connectivity *in vivo*.

Discussion

Differential control of cortical axonogenesis and dendritogenesis by activation of CaMKIα and CaMKIγ/CL3

In a previous work (Takemoto-Kimura et al., 2007), we showed that a lipid-modified CaM kinase CaMKIγ/CL3 (a membrane-anchored CaMKI isoform) was directed to the dendrites on raft insertion and could potently promote early dendritic development, with little effect on axon outgrowth, in cultured cortical neurons. In striking contrast to CaMKIγ/CL3, we here demonstrate that a cytosolic sister kinase, CaMKIα, has a complementary role: it has little role in dendritogenesis, but is necessary and sufficient to promote axonogenesis in the same preparation. Additionally, our present work established that CaMKIα regulates axonal extension *in vivo*. Additional rigorous quantitative studies are awaited to establish the potential role of other CaMKK–CaMK signaling pathways in cortical neuritogenesis in general.

How can such specificity of axonal/dendritic growth be regulated by two separate yet structurally resembling kinases lying downstream of the same CaMKKs? The chimeric kinase experiments (Fig. 4) strongly suggested that the diverging kinase substrate specificities and the dissimilarity in subcellular localization (cytosol vs dendritic rafts) might provide a basis for the strikingly differential effect of CaMKIα and CaMKIγ/CL3 during axonal and dendritic development. In support of this functional segregation between the two distinct CaMKK–CaMKI cascades, we identified an extracellular ligand, GABA, which specifically stimulated axonal growth via CaMKIα (this study), whereas BDNF selectively promoted dendritic growth via CaMKIγ (Takemoto-Kimura et al., 2007), during an early developmental stage of cortical neurons.

In principle, BDNF could rather selectively act on dendrites in part because of the strong affinity of the active TrkB receptor to lipid rafts (Suzuki et al., 2004), which are enriched on dendrites. At this point, however, how GABA stimuli could possibly generate an axon-specific effect remains rather unclear, although preliminary Ca^{2+} imaging experiments indicated that $GABA_A$ stimulation might trigger growth cone-localized Ca^{2+} transients (S. Kamijo, H. Fujii, S. Takemoto-Kimura, and H. Bito, unpublished data). It is noteworthy that many potential *in vitro* substrates of CaMKIα have previously been associated with axonal or presynaptic functions. These include synapsin I (Nairn and Greengard, 1987), Numb and Numbl (Tokumitsu et al., 2005), microtubule affinity regulating kinase 2 (MARK2/Par-1b) (Uboha et al., 2007), and β-Pak-interacting exchange factor (βPIX) (Saneyoshi et al., 2008). Although some of these known substrates of CaMKI may potentially underlie a part of early axonal growth, additional work is clearly needed to fully elucidate how an axonogenic substrate may be activated via phosphorylation by CaMKIα.

A pivotal role for a GABA-driven CaMKK–CaMKIα cascade in controlling axonal morphogenesis during early development

In this work, we identified a crucial role for GABA in controlling cortical axon outgrowth during early development via a CaMKK–CaMKIα cascade. In immature cortical neurons, what is the mechanism by which GABA can stimulate axonal development in a CaMKI-dependent manner? Recent studies showed that $GABA_A$ receptors activation has potent excitatory effects in immature, but not in mature, neurons (Ben-Ari et al., 2007). The excitatory action of GABA was demonstrated to be caused by a high basal Cl^- concentration in immature neurons, because of a high amount of the Na^+–K^+–$2Cl^-$ cotransporter (NKCC1) which favors Cl^- influx, whereas the K^+–Cl^- cotransporter (KCC2) primarily responsible for Cl^- efflux is still low in expression (Payne et al., 2003). Because of elevated intracellular Cl^- concentration in immature neurons, $GABA_A$ receptors activation thus induces depolarization (Ben-Ari et al., 2007), thereby likely triggering the opening of voltage-gated Ca^{2+} channels, which then generates enough Ca^{2+} influx leading to CaMKK–CaMKIα activation.

During early development, it is now known that GABA controls a variety of biological processes. Our work has only addressed the significance of the CaMKK–CaMKIα cascade in GABA-mediated cortical axonogenesis during the perinatal period. Whether other GABA-regulated processes may also be mediated by CaMKIα clearly remains to be investigated. For instance, the process of cortical migration has also been reported to be regulated by GABA through signal transduction pathways involving Ca^{2+}, both *in vitro* (Behar et al., 1996, 1998, 2000) and *in vivo* (Heck et al., 2007). Interestingly, treatment with calmidazolium, an inhibitor of calmodulin, reduces the migration rate in cerebellar granule cells (Kumada and Komuro, 2004). Additional studies are needed to determine whether the CaMKK–CaMKIα cascade may play additional roles in such developmental processes as well.

A CaMKK–CaMKIα pathway may regulate fine-sculpting of cortical wiring

We here established the critical importance of an axonogenic GABA–CaMKK–CaMKIα pathway during early development *in vitro*. Moreover, this study indicated that CaMKIα regulated activity-dependent extension of terminal cortical axons *in vivo*. Interestingly, premature elimination of excitatory GABA action by forced expression of KCC2 in newly born cortical neurons dramatically perturbed the morphological maturation of the dendrites (Cancedda et al., 2007) or of the terminal callosal axon branches (H. Mizuno, T. Hirano, and Y. Tagawa, unpublished data). Our present findings thus uncover an unexpected role of the CaMKK–CaMKIα cascade as one key mechanism in GABA-driven activity-dependent regulation of cortical connectivity. More studies are needed to establish whether and how other Ca^{2+}-mobilizing signals (e.g., BDNF) may spatially and temporally interact and perhaps cooperate with such an axonogenic GABA–CaMKK–CaMKIα pathway. Finally, our data lend support to the existence of a perinatal time window of structural refinement, during which spontaneous Ca^{2+} signaling regulated by trophic factors, guidance signals, and ambient neurotransmitters, such as BDNF or GABA, critically fine-tunes cortical connectivity, perhaps even before the receipt of the earliest sensory cues.

References

Behar TN, Li YX, Tran HT, Ma W, Dunlap V, Scott C, Barker JL (1996) GABA stimulates chemotaxis and chemokinesis of embryonic cortical neurons via calcium-dependent mechanisms. J Neurosci 16:1808–1818.

Behar TN, Schaffner AE, Scott CA, O'Connell C, Barker JL (1998) Differential response of cortical plate and ventricular zone cells to GABA as a migration stimulus. J Neurosci 18:6378–6387.

Behar TN, Schaffner AE, Scott CA, Greene CL, Barker JL (2000) GABA receptor antagonists modulate postmitotic cell migration in slice cultures of embryonic rat cortex. Cereb Cortex 10:899–909.

Ben-Ari Y, Gaiarsa JL, Tyzio R, Khazipov R (2007) GABA: a pioneer transmitter that excites immature neurons and generates primitive oscillations. Physiol Rev 87:1215–1284.

Bito H, Takemoto-Kimura S (2003) Ca^{2+}/CREB/CBP-dependent gene regulation: a shared mechanism critical in long-term synaptic plasticity and neuronal survival. Cell Calcium 34:425–430.

Bito H, Deisseroth K, Tsien RW (1996) CREB phosphorylation and dephosphorylation: a Ca^{2+}- and stimulus duration-dependent switch for hippocampal gene expression. Cell 87:1203–1214.

Blaeser F, Sanders MJ, Truong N, Ko S, Wu LJ, Wozniak DF, Fanselow MS, Zhuo M, Chatila TA (2006) Long-term memory deficits in pavlovian fear conditioning in Ca^{2+}/calmodulin kinase kinase alpha-deficient mice. Mol Cell Biol 26:9105–9115.

Cancedda L, Fiumelli H, Chen K, Poo MM (2007) Excitatory GABA action is essential for morphological maturation of cortical neurons *in vivo*. J Neurosci 27:5224–5235.

Dickson BJ (2002) Molecular mechanisms of axon guidance. Science 298:1959–1964.

Furuyashiki T, Arakawa Y, Takemoto-Kimura S, Bito H, Narumiya S (2002) Multiple spatiotemporal modes of actin reorganization by NMDA receptors and voltage-gated Ca^{2+} channels. Proc Natl Acad Sci U S A 99:14458–14463.

Gomez TM, Zheng JQ (2006) The molecular basis for calcium-dependent axon pathfinding. Nat Rev Neurosci 7:115–125.

Heck N, Kilb W, Reiprich P, Kubota H, Furukawa T, Fukuda A, Luhmann HJ (2007) GABA-A receptors regulate neocortical neuronal migration in vitro and in vivo. Cereb Cortex 17:138–148.

Hook SS, Means AR (2001) Ca^{2+}/CaM-dependent kinases: from activation to function. Annu Rev Pharmacol Toxicol 41:471–505.

Hudmon A, Schulman H (2002) Neuronal Ca^{2+}/calmodulin-dependent protein kinase II: the role of structure and autoregulation in cellular function. Annu Rev Biochem 71:473–510.

Ishikawa Y, Tokumitsu H, Inuzuka H, Murata-Hori M, Hosoya H, Kobayashi R (2003) Identification and characterization of novel components of a Ca^{2+}/calmodulin-dependent protein kinase cascade in HeLa cells. FEBS Lett 550:57–63.

Kater SB, Mattson MP, Cohan C, Connor J (1988) Calcium regulation of the neuronal growth cone. Trends Neurosci 11:315–321.

Kumada T, Komuro H (2004) Completion of neuronal migration regulated by loss of Ca^{2+} transients. Proc Natl Acad Sci U S A 101:8479–8484.

Mizuno H, Hirano T, Tagawa Y (2007) Evidence for activity-dependent cortical wiring: formation of interhemispheric connections in neonatal mouse visual cortex requires projection neuron activity. J Neurosci 27:6760–6770.

Nairn AC, Greengard P (1987) Purification and characterization of Ca^{2+}/calmodulin-dependent protein kinase I from bovine brain. J Biol Chem 262:7273–7281.

Nonaka M, Doi T, Fujiyoshi Y, Takemoto-Kimura S, Bito H (2006) Essential contribution of the ligand-binding βB/βC loop of PDZ1 and PDZ2 in the regulation of postsynaptic clustering, scaffolding, and localization of postsynaptic density-95. J Neurosci 26:763–774.

Owens DF, Boyce LH, Davis MB, Kriegstein AR (1996) Excitatory GABA responses in embryonic and neonatal cortical slices demonstrated by gramicidin perforated-patch recordings and calcium imaging. J Neurosci 16:6414–6423.

Payne JA, Rivera C, Voipio J, Kaila K (2003) Cation-chloride co-transporters in neuronal communication, development and trauma. Trends Neurosci 26:199–206.

Represa A, Ben-Ari Y (2005) Trophic actions of GABA on neuronal development. Trends Neurosci 28:278–283.

Rivera C, Voipio J, Payne JA, Ruusuvuori E, Lahtinen H, Lamsa K, Pirvola U, Saarma M, Kaila K (1999) The K^+/Cl^- co-transporter KCC2 renders GABA hyperpolarizing during neuronal maturation. Nature 397:251–255.

Saneyoshi T, Wayman G, Fortin D, Davare M, Hoshi N, Nozaki N, Natsume T, Soderling TR (2008) Activity-dependent synaptogenesis: regulation by a CaM-kinase kinase/CaM-kinase I/betaPIX signaling complex. Neuron 57:94–107.

Schmitt JM, Wayman GA, Nozaki N, Soderling TR (2004) Calcium activation of ERK mediated by calmodulin kinase I. J Biol Chem 279:24064–24072.

Soderling TR (1999) The Ca-calmodulin-dependent protein kinase cascade. Trends Biochem Sci 24:232–236.

Soderling TR, Stull JT (2001) Structure and regulation of calcium/calmodulin-dependent protein kinases. Chem Rev 101:2341–2352.

Suzuki S, Numakawa T, Shimazu K, Koshimizu H, Hara T, Hatanaka H, Mei L, Lu B, Kojima M (2004) BDNF-induced recruitment of TrkB receptor into neuronal lipid rafts: roles in synaptic modulation. J Cell Biol 167:1205–1215.

Takemoto-Kimura S, Terai H, Takamoto M, Ohmae S, Kikumura S, Segi E, Arakawa Y, Furuyashiki T, Narumiya S, Bito H (2003) Molecular cloning and characterization of CLICK-III/CaMKIgamma, a novel membrane-anchored neuronal Ca^{2+}/calmodulin-dependent protein kinase (CaMK). J Biol Chem 278:18597–18605.

Takemoto-Kimura S, Ageta-Ishihara N, Nonaka M, Adachi-Morishima A, Mano T, Okamura M, Fujii H, Fuse T, Hoshino M, Suzuki S, Kojima M, Mishina M, Okuno H, Bito H (2007) Regulation of dendritogenesis via a lipid-raft-associated Ca^{2+}/calmodulin-dependent protein kinase CLICK-III/CaMKIgamma. Neuron 54:755–770.

Tessier-Lavigne M, Goodman CS (1996) The molecular biology of axon guidance. Science 274:1123–1133.

Tokumitsu H, Inuzuka H, Ishikawa Y, Ikeda M, Saji I, Kobayashi R (2002) STO-609, a specific inhibitor of the Ca^{2+}/calmodulin-dependent protein kinase kinase. J Biol Chem 277:15813–15818.

Tokumitsu H, Inuzuka H, Ishikawa Y, Kobayashi R (2003) A single amino acid difference between alpha and beta Ca^{2+}/calmodulin-dependent protein kinase kinase dictates sensitivity to the specific inhibitor, STO-609. J Biol Chem 278:10908–10913.

Tokumitsu H, Hatano N, Inuzuka H, Sueyoshi Y, Yokokura S, Ichimura T, Nozaki N, Kobayashi R (2005) Phosphorylation of Numb family proteins. Possible involvement of Ca^{2+}/calmodulin-dependent protein kinases. J Biol Chem 280:35108–35118.

Uboha NV, Flajolet M, Nairn AC, Picciotto MR (2007) A calcium- and calmodulin-dependent kinase Iα/microtubule affinity regulating kinase 2 signaling cascade mediates calcium-dependent neurite outgrowth. J Neurosci 27:4413–4423.

Uezu A, Fukunaga K, Kasahara J, Miyamoto E (2002) Activation of Ca^{2+}/calmodulin-dependent protein kinase I in cultured rat hippocampal neurons. J Neurochem 82:585–593.

Wang CL, Zhang L, Zhou Y, Zhou J, Yang XJ, Duan SM, Xiong ZQ, Ding YQ (2007) Activity-dependent development of callosal projections in the somatosensory cortex. J Neurosci 27:11334–11342.

Wang DD, Kriegstein AR (2008) GABA regulates excitatory synapse formation in the neocortex via NMDA receptor activation. J Neurosci 28:5547–5558.

Wayman GA, Kaech S, Grant WF, Davare M, Impey S, Tokumitsu H, Nozaki N, Banker G, Soderling TR (2004) Regulation of axonal extension and growth cone motility by calmodulin-dependent protein kinase I. J Neurosci 24:3786–3794.

Wayman GA, Impey S, Marks D, Saneyoshi T, Grant WF, Derkach V, Soderling TR (2006) Activity-dependent dendritic arborization mediated by CaM-kinase I activation and enhanced CREB-dependent transcription of Wnt-2. Neuron 50:897–909.

Yokokura H, Terada O, Naito Y, Hidaka H (1997) Isolation and comparison of rat cDNAs encoding Ca^{2+}/calmodulin-dependent protein kinase I isoforms. Biochim Biophys Acta 1338:8–12.

frontiers in
BEHAVIORAL NEUROSCIENCE

ORIGINAL RESEARCH ARTICLE
published: 14 August 2009
doi: 10.3389/neuro.08.012.2009

Litter environment affects behavior and brain metabolic activity of adult knockout mice

***David Crews*[1]*, *David Rushworth*[1], *Francisco Gonzalez-Lima*[2] *and Sonoko Ogawa*[3]**

[1] *Section of Integrative Biology, University of Texas at Austin, Austin, TX, USA*
[2] *Institute of Neuroscience and the Department of Psychology, University of Texas at Austin, Austin, TX, USA*
[3] *Laboratory of Behavioral Neuroendocrinology, Graduate School of Comprehensive Human Sciences, University of Tsukuba, Ibaraki, Japan*

Edited by:
Larry J. Young, Emory University, USA; Yerkes National Primate Research Center, USA

Reviewed by:
Lance Kriegsfeld, University of California, USA
Emily Rissman, University of Virginia, USA

***Correspondence:**
David Crews, Section of Integrative Biology, University of Texas at Austin, Austin, TX 78712, USA.
e-mail: crews@mail.utexas.edu

In mammals, the formative environment for social and anxiety-related behaviors is the family unit; in the case of rodents, this is the litter and the mother-young bond. A deciding factor in this environment is the sex ratio of the litter and, in the case of mice lacking functional copies of gene(s), the ratio of the various genotypes in the litter. Both Sex and Genotype ratios of the litter affect the nature and quality of the individual's behavior later in adulthood, as well as metabolic activity in brain nuclei that underlie these behaviors. Mice were raised in litters reconstituted shortly after to birth to control for sex ratio and genotype ratio (wild type pups versus pups lacking a functional estrogen receptor α). In both males and females, the Sex and Genotype of siblings in the litter affected aggressive behaviors as well as patterns of metabolic activity in limbic nuclei in the social behavior network later in adulthood. Further, this pattern in males varied depending upon the Genotype of their brothers and sisters. Principal Components Analysis revealed two components comprised of several amygdalar and hypothalamic nuclei; the VMH showed strong correlations in both clusters, suggesting its pivotal nature in the organization of two neural networks.

Keywords: life history, sex differences, genotype differences, sibling, aggression

INTRODUCTION

Adult sociosexual behavior is the cumulative result of genetics and experience. These experiences begin prenatally in the intrauterine environment, and continue in early postnatal life according to litter composition and maternal behavior, influencing how the individual interacts with the social environment in adulthood (Crews, 1999; Crews and Groothuis, 2005; Fleming et al., 2002; Meaney, 2001; Moore, 1995; Moore et al., 1997; Sakata et al., 2001). Various studies indicate that experiences can be imprinted epigenetically to influence future generations (Bateson, 2005; Crews, 2008; Crews et al., 2007; Crews and McLachlan, 2006; Gottlieb, 2002; Jablonka and Lamb, 1995; Lewontin, 2000; Waddington, 1942, 1953; West-Eberhard, 2003).

Complex behaviors such as aggressive, affiliative behaviors, and anxiety-related behaviors depend upon concerted interaction of many brain nuclei acting together, not in isolation. Extensive research has revealed that specific nuclei involved in the regulation of behavior are reciprocally interconnected, often express receptors for steroid hormones, and function in concert as a neural network. Newman (1999) proposed that behavioral traits depend ultimately upon this social behavior network. Behavioral traits depend ultimately upon the ability of this network(s) of nuclei and neurons to sustain a certain level of metabolic activity necessary for interaction. Of particular interest is how these nuclei might be functionally associated in the adult, and how early environment might change these functional associations. A method that enables study of the long-term consequences of life history changes is cytochrome oxidase IV (COX) quantitative enzyme histochemistry (Sakata et al., 2005). COX, complex IV of the mitochondrial respiratory chain, the rate-limiting enzyme for the production of utilizable energy derived by coupling oxidative metabolism to the production of ATP. Thus, the abundance of COX serves as an endogenous marker of metabolic capacity in nuclei and neurons, portraying the result of long-term metabolic demand as well as the capacity of a network of nuclei to support specific behaviors. Previous work with rodents reveals that early experience (both pre- and postnatal) significantly affects COX activity in the adult limbic forebrain nuclei and that early experience can modify functional associations of nuclei within integrated neural circuits (c.f., Crews et al., 2006; Jones et al., 1997; Sakata et al., 2002).

In behavioral research with rodents in general, and genetically modified mice in particular, the sex and/or genotype ratios of the

Abbreviations: ♀WT, female wildtype mouse; ♀KO, female estrogen receptor a knockout mouse; ♂WT, male wildtype mouse; ♂KO, male estrogen receptor a knockout mouse; ACo, anterior cortical amygdaloid nucleus; AHA, anterior hypothalamic area, anterior; AVPe, anteroventral periventricular nucleus (=AVPV); BST, bed nucleus of the stria terminalis, including anterior and lateral ventral divisions; BSTMA, bed nucleus of the stria terminalis medial division, anterior; BSTMPM, bed nucleus of the stria terminalis, medial division, posteromedial; CeA, central amygdaloid nucleus; CLC, caudal limbic cluster; cMPOA, caudal medial preoptic area; CO, cytochrome c oxidase, complex IV, EC 1.9.3.1; ERα, estrogen receptor α; KO, ERα knockout; LHb, lateral habenular nucleus; LSI, lateral septal nucleus intermediate; MeAA, medial amygdaloid (MeA) nucleus, anterior; MeAPD, medial amygdaloid (MeA) nucleus, posterodorsal; MeAPV, medial amygdaloid (MeA) nucleus, posteroventral; MHb, medial habenular nucleus; MPOA, medial preoptic area; PaN, paraventricular hypothalamic nucleus; PC, principal component; Pe, periventricular hypothalamic nucleus; RLC, rostral limbic cluster; rMPOA, rostral medial preoptic area; VMH, ventromedial hypothalamic nucleus, including rostral and central VMH; VMHDM, ventromedial hypothalamic nucleus, dorsomedial; VMHVL, ventromedial hypothalamic nucleus, ventrolateral.

litter in which individuals are reared are often ignored. Previous research with estrogen receptor α knockout (ERKO) mice suggests that litter composition influences the sociosexual behaviors of these KO mice in adulthood (Crews et al., 2004). Namely, when Genotype is considered as a component of litter composition, behavioral differences between the Genotypes are more sharply defined and less variable than reported previously. The present study utilized the same paradigm as described in Crews et al. (2004). Thus, pups derived from mating males and females heterozygous (HTZ) for a null mutation of estrogen receptor α (ERα) were sexed and genotyped within 2 days after birth. With this information litters were reconstituted, forming either same-sex/same-genotype controls, same-sex/mixed-genotype litters of equal numbers of KO and wildtype (WT) individuals, mixed-sex/same-genotype, or mixed-sex/mixed-genotype litters of equal numbers of male or female young.

We hypothesized that behavioral variations caused by genetic and developmental factors within the litter environment correlate with differences in behavior and COX activity in specific brain areas later in adulthood. Using genetically-modified mice we demonstrate that the sex and genotype ratio of the litter has a powerful effect on the organization of the neural mechanisms controlling social and anxiety-related behaviors.

MATERIALS AND METHODS

MICE

Mice were produced by mating male and nulliparous female mice HTZ for a dysfunctional ERα gene, which were backcrossed to C57B/6J mice. These mice were obtained from the breeding colony maintained at Rockefeller University. Two to three females were housed with a male, and, when they were visibly pregnant (3–5 days before the day of delivery based on *post hoc* analyses), they were singly housed. Animal rooms were maintained on a 12:12 h Light:Dark cycle at constant temperature (22°C) with food (PicoLab Rodent Diet 20, Oakville, ON, Canada) and water available *ad libitum*. All procedures were approved by the Rockefeller University, University of Tsukuba, and University of Texas Animal Use and Care Committees.

All pups were sexed and genotyped within 2 days of birth and the litters re-constituted on PND 2. During this period, each pup received individual identification marks on the body by a Sharpie™ permanent marker, a procedure that was repeated each day. After genotyping, individuals were identified with individually specific toe clips for permanent identification. In all instances, HTZ females that had contributed young to the study served as foster mothers.

Littermates were separated in a systematic manner to insure that litter source was not overrepresented in each group. Pups were reared in litters of four; all individuals survived to weaning. As in previous studies with these animals, individuals continued to be group-housed with littermates of the same sex and genotype following weaning. Unlike previous studies, individuals were housed according to genotype (e.g., ♂WT with only ♂WT) after weaning. Two weeks before behavior testing, all animals were individually housed. Behavioral testing began at approximately 8 weeks of age for all mice and included tests of anxiety (Light:Dark transition test) and of social and aggressive behaviors (resident-intruder test) in this order. All animal husbandry, testing, and euthanasia followed approved institutional IACUC guidelines and NIH Guidelines for the Use of Animals in Research.

RECONSTITUTION OF LITTERS

Two separate studies were performed, one focusing on males and the other on females. Experimental litters were reconstituted from natal litters into one of 16 possible combinations: same-sex, same-genotype; same-sex, mixed-genotype; mixed-sex, same-genotype; mixed-sex, mixed-genotype totaling more than 450 pups. Only four litter types of the 16 possible combinations were impossible to construct in adequate sample sizes and so the present report is limited to the 12 litter types that were reconstituted in sufficient sample sizes for statistical analysis. **Table 1** details the distribution of a male or a female animals' genotype (experimental cohort) with respect to the sex and genotype of the other half of the animals in the litter (Sibling Type) along with the number of litters from each of these groups. The number of individuals and experimental litters reconstituted from natal litters totaled were as follows: for males, a total of 200 individuals divided into 39 same-sex, and 22 mixed-sex litters; for females, a total of 168 individuals divided into 42 same-sex, and 13 mixed-sex litters.

As adults an individual of each sex and genotype from the experimental cohort was chosen at random from each of the litters and tested for anxiety and affiliative behaviors. Another individual was selected at random for the COX histochemistry. Hence individuals used for assessment of brain metabolic activity were not tested before sacrifice, but were the same age as those individuals that were tested.

BEHAVIORAL TESTING

Light:Dark transition test

The test apparatus consisted of clear plastic box (50 cm × 50 cm × 35 cm) and a black (light opaque) covered-plastic box (50 cm × 25 cm × 25 cm) was inserted in one side (the dark side). The black box had an open doorway (2 cm × 5 cm) that led to the light side of the apparatus, which was illuminated by a 40-W white bulb. Mice were moved from the living room to the experimental room at least 1 h before the test. At the beginning of the tests, mice were removed from their cages, gently placed at the doorway, and released into the dark side of the apparatus (Ogawa et al., 2003, 2005). A Digiscan analyzer and software (Omnitech Electronics Inc., Dartmouth, NS,

Table 1 | Sex and genotype combinations in reconstituted litters from mating mice heterozygous for estrogen receptor α (WT, wildtype; KO, knockout). The "individual" rows indicate the experimental cohort (mice in which dependent variables were measured) while the columns "Sibling Type" indicates the stimulus cohort (siblings used as independent variables). All litters consisted of four individuals. A single individual from each litter was used in the behavioral studies and another used for cytochrome oxidase histochemistry.

	Sibling type			
Individual	**♂WT**	**♂KO**	**♀WT**	**♀KO**
♂WT	11	7	7	6
♂KO	11	10	NA	NA
♀WT	11	NA	17	11
♀KO	11	NA	8	6

NA means not available as the number of litters created for these groups did not reach the minimum required of six.

Canada) were used to collect and store horizontal-activity, which was monitored by infrared beams. For each mouse, total activity (total number of beam breaks) and cumulative time spent in each compartment were recorded during 10 min tests. Gonadally intact male and female mice were tested once at 8 weeks of age.

Resident-intruder test

To determine if litter composition influences affiliative behavior in adulthood, mice were tested in a resident-intruder paradigm as in previous studies from this laboratory (Ogawa et al., 1996, 1997, 1998a,b). All individuals were gonadally intact. In females, the stage of estrous cycle at the time of testing was not determined for experimental females. Behavior tests lasted for 15 min during the dark phase (4–8 h after lights off) under red light. Experimental males were tested with olfactory bulbectomized C57BL/6J male intruders and females were tested with ovariectomized C57BL/6J female intruders. Cumulative duration of social interaction including sniffing, genital licking, and grooming was recorded for each experimental mouse. Experimental males and females were tested on two consecutive days at 9 weeks of age.

STATISTICS FOR BEHAVIORAL MEASURES

Behavioral data were analyzed after they were log-transformed, if necessary, so as to normalize the distributions and remove non-homogeneity. They were then analyzed for group differences of each sex by ANOVAs followed by *t*-test *post hoc* analyses.

TISSUE PREPARATION AND CYTOCHROME OXIDASE IMAGING

Brains were removed immediately following decapitation and prepared for COX imaging as per Gonzalez-Lima and Cada (1998). The same individual measured all of the areas after extensive training in neuroanatomy. All measures were done blind, the key being broken only after the completion of all measurements.

For the purposes of comparing COX activity between each batch, a two-way ANOVA was performed using whole brain (WB) measures that were partitioned into the factors of three anatomical regions and into the batches in which these brains were stained. The three anatomical regions (rostral, medial, and caudal) as well as the nuclei measured are depicted in **Figure 1**. Testing the arbitrary subdivisions of the mouse brain with a small representative random sample of the study population ($n = 12$) indicated that further subdivision of WB regions from the original subdivisions did not yield significant regional effects on individual nuclei activity after normalization (two-way ANOVA, $F = 0.845$, df = 9, $p = 0.575$). This finding suggests that subdivision into three regions is sufficient to capture the regional variation in WB activity. Normalization is used to correct for observed staining variability and allow comparisons between different groups of animals or nuclei. For normalization, the average COX activity of a given nucleus was divided by the respective averaged regional WB COX activity for each individual to generate this value for normalized nucleus activity. This correction was made for all nuclei in the entire population of experimental animals and was used in all subsequent analyses other than ANOVA comparisons; in the latter instance a two-way ANOVA was performed for the factors of Genotype and Sex for WB activity and for each of the 20 nuclei using Hochberg's GT2 *post hoc* analysis.

PRINCIPAL COMPONENTS ANALYSIS

Data reduction performed with principal component (PC) analysis was used to decompose the full set of all nuclei influences between one another into eigenvectors or PCs that selected a few nuclei that were contributing to most of the variance. In this study, PCs were

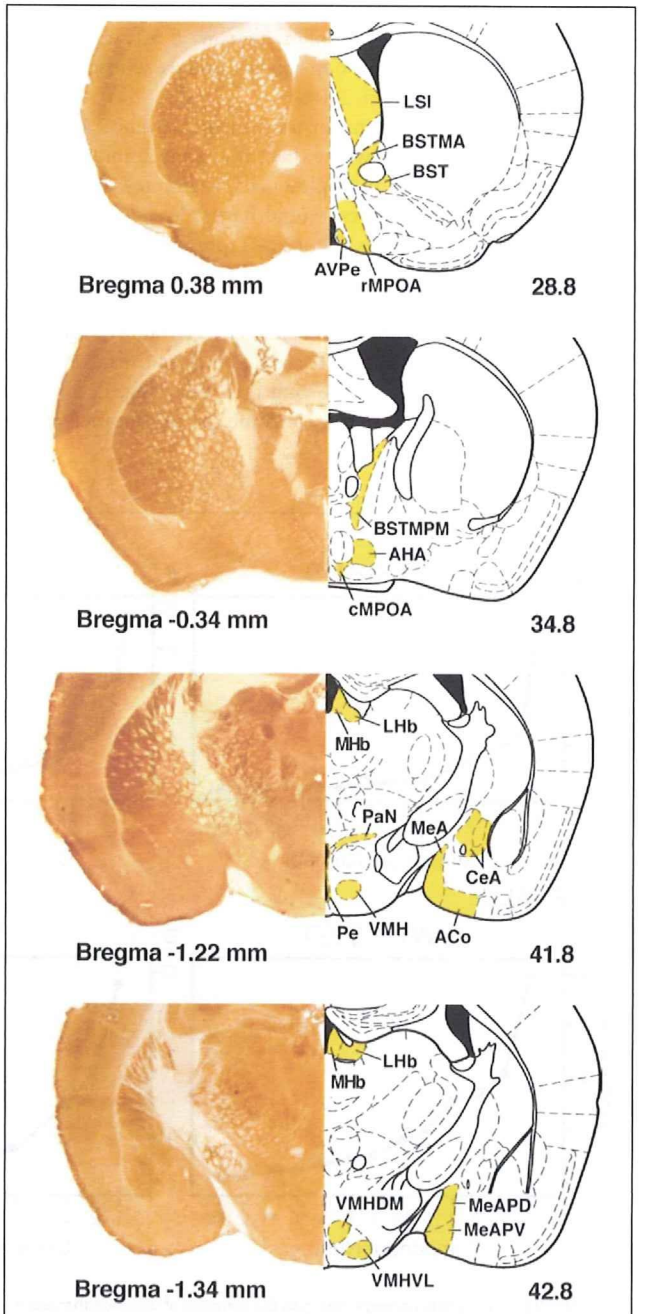

FIGURE 1 | Left column is a composite of sample mouse brain images histochemically stained for cytochrome oxidase with immediate right column delineating the boundaries of nuclei measured in yellow in the corresponding coronal sections in Paxinos and Franklin (2001); the bottom left number refers to Bregma and the bottom right number refers to the figure number.

derived in iteratively repeated attempts to account for as much of the variance in the original correlation matrix as possible, with each subsequent PC accounting for less variance than the PC before it. A plot of these ordered eigenvalues is called a SCREE plot, and can be used to help visually interpret the following criteria for the significance of a PC as outlined by Ecker et al. (2007) (**Figure 2**):

(1) Kaiser's rule, stated in the following way: $l^2 > 1$, was used to find PCs that account for non-trivial variance within the correlation matrix (Loehlin, 2004).
(2) If only a few PCs account for most of the variance, as would be expected in the case where there was some amount of shared variance between multiple nuclei, then a few PCs would have a high l^2 and the rest would have a low l^2. If one PC's eigenvalue l_n^2, where n is the index representing the ordered occurrence of each PC, accounts for more variance than the following PCs, then $(l_n^2 - l_{n+1}^2)$ – the difference between the large eigenvalue and the subsequent smaller eigenvalue – should be large in comparison to the difference between the next pair of eigenvalues $(l_{n+1}^2 - l_{n+2}^2)$. Following this reasoning, Ecker et al. (2007) used Equation 1 to determine the significance of the nth PC:

$$\frac{l_n^2 - l_{n+1}^2}{l_{n+1}^2 - l_{n+2}^2} \geq 3.0 \quad (1)$$

Each time that this equation is true, a significant drop in the eigenvalues has occurred, and should correspond to a large drop on the SCREE plot.
(3) Only eigenvalues occurring before the end of the first series of large drops in the SCREE plot are considered significant. This is also called the elbow criterion after Catell (1966) for reasons that become apparent when viewing **Figure 2**.

Principal components analysis (PCA) was used to derive PCs from a data set containing all males ($n = 37$) and later all females ($n = 34$) in their respective studies that had no missing values for a given set of nuclei used in their analyses. The analysis was also used on each sex for subsets of each of the genotypes used in the analysis. In all, PC analysis was performed three times for each sex: once for all animals in the parsed data set, again for the WT, and then KO within those data sets. After the significant PCs for each group were determined, the coefficients of each nucleus for the significant PCs were checked against the following criterion: if the value of the coefficient was found to be greater than 0.60, then the nucleus

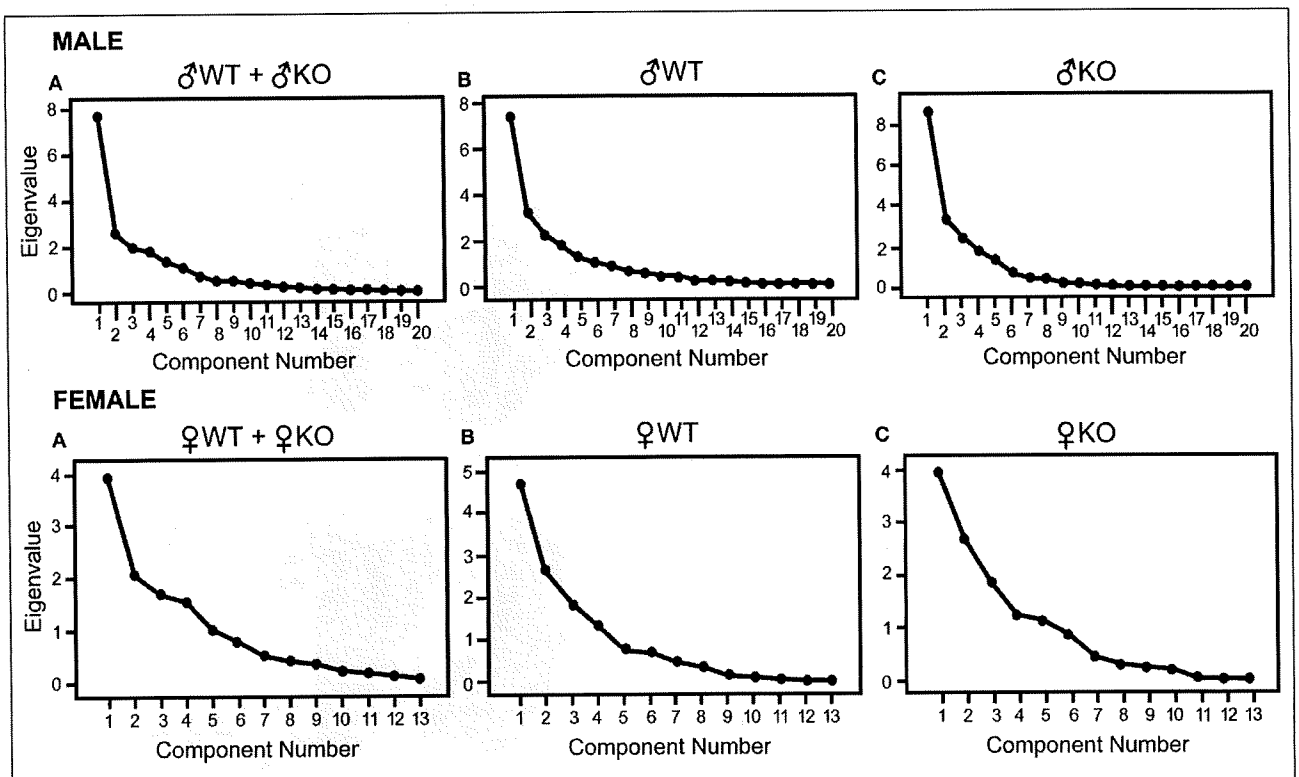

FIGURE 2 | SCREE plots corresponding to the amount of variance that each eigenvalue accounts for. The largest point on the left of each plot is the eigenvalue representing the first principal component derived, which is the first in an iterative process of attempting to account for as much variance as possible in the correlation matrix and its subsequent residual matrices. A precipitous slope, as seen in each SCREE plot, indicates that the amount of variance accounted for by the following component is not nearly as great as the previous. This observation is the basis of Eq. 1. For males each plot shows a main component and a few less significant components that quickly become trivial (triviality is $\lambda^2 < 1$, see **Table 4**), indicating that among the 20 nuclei considered there is an underlying group of nuclei that is primarily driving the strength of the correlation matrix. Females show a less steep slope. Eigenvalues shown in SCREE plots were derived using principal component analysis for males on the top row and females on the bottom. Top row: **(A)**: all males (♂WT + ♂KO; $n = 37$), **(B)**: ♂WT only ($n = 21$), and **(C)**: ♂KO only ($n = 16$). Bottom row: **(A)**: all females (♀WT + ♀KO; $n = 34$), **(B)**: ♀WT only ($n = 17$), and **(C)**: ♀KO only ($n = 17$).

of that coefficient is placed into a set of nuclei for further analysis using Pearson's bivariate correlation along with the jackknifing procedure. All nuclei found significant in a single PC were considered independently of the nuclei considered in another PC unless the same nuclei occurred with a coefficient greater than 0.60 in both PCs; this rule had one exception during analysis of the male tissue that served as a control. The coefficient value used in this analysis was selected for its ability to separate nuclei into smaller groups that did not have a large number of shared nuclei and following the observation that nuclei values below this coefficient were often much lower (0.00–0.30) than the value of 0.6.

INTER-REGIONAL CORRELATIONS IN METABOLIC ACTIVITY

Each nucleus selected from a given PC was subjected to a modified jackknifing procedure similar to that used by Sakata et al. (2000) to find correlations that were consistently significant between nuclei. To find group differences when appropriate, groups were segregated into subsets of the full data set depending upon an experimental factor (i.e., Genotype or Sibling Type) and then subjected to the jackknifing procedure. Correlations found to be significant after jackknifing in multiple groups were tested for a statistically significant difference in correlations between groups. This was done by taking the correlation coefficient from each $n-1$ step in the jackknifing procedure and comparing this set of correlations with the equivalent correlations in the comparison group using the *t*-test with assumed unequal variance.

LIMBIC LANDSCAPES

For visualization of how discrete nuclei are modified by the litter environment, the limbic landscape method described in Crews et al. (2006) was utilized.

RESULTS

BEHAVIOR: MALES

Resident-intruder test

Aggression in male mice was significantly influenced by both the Sex and Genotype of the littermates (**Figure 3A**). When raised in litters having either ♂KO or ♀KO littermates, ♂WT were more aggressive than when raised in litters containing either ♂WT or ♀WT littermates. KO males were not aggressive when raised in litters containing either ♂KO or ♂WT littermates.

Light:Dark transition test

The cumulative duration spent in the light compartment was significantly increased in ♂WT mice raised with ♀WT littermates, but not when raised with ♀KO littermates (**Figure 4**). The latency to move to the light compartment was increased by the presence of ♂KO or ♀KO pups in the litter, but not when the littermates were ♀WT or ♂WT.

BEHAVIOR: FEMALES

Resident-intruder test

Overall, ♀KO reared only with ♀KO sisters showed significantly less social contact in the resident-intruder test compared to ♀WT raised with ♀WT sisters or when raised with ♀KO or ♂WT littermates (**Figure 3B**). Social contact time in ♀KO mice was increased by the presence of ♂WT brothers or ♀WT sisters in the litter; although in the latter instance ♀KO were not significantly from those raised with ♀KO sisters. In contrast, ♀KO raised with ♂WT brothers were not different from ♀WT regardless of litter type.

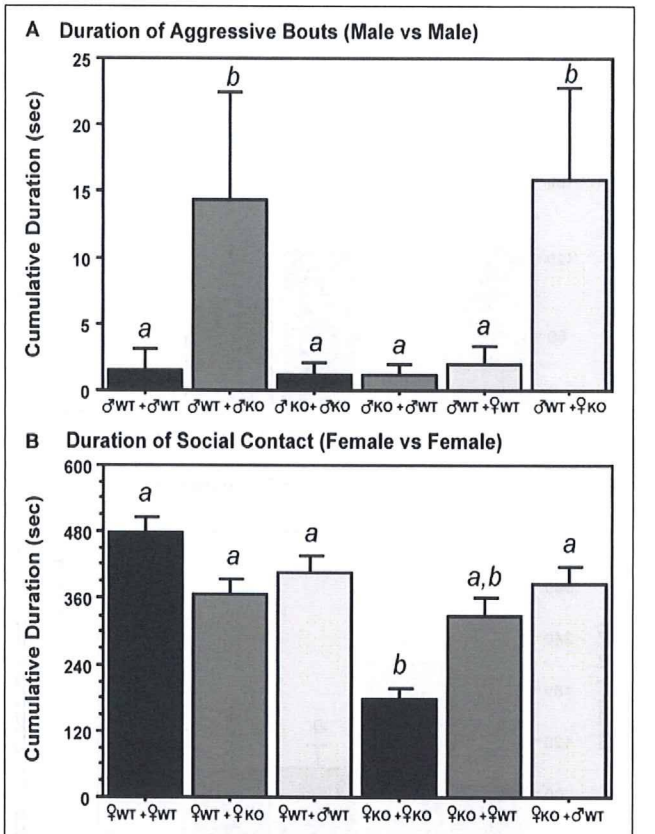

FIGURE 3 | Litter composition affects the sociosexual behaviors of adult male and female estrogen receptor α knockout (ERKO) mice. **(A)** Represents the duration (seconds) of aggressive bouts exhibited by male mice in resident-intruder tests. **(B)** Represents the duration seconds) of social contact exhibited by females in resident-intruder tests. Mean and SE is indicated; letters above bars indicate significant differences.

Light:Dark transition test

There were no significant differences among females according to the Sex or Genotype of their littermates.

CYTOCHROME OXIDASE ACTIVITY: MALES

There was a significant effect ($p < 0.01$) on WB activity due to Sibling Type but not to Genotype or an interaction between the Sibling Type and Genotype (**Table 2**). Further analysis (two-way ANOVA with WB region and Sibling Type as main factors) indicated no significant effect of Sibling Type on interaction between regional WB activity and Sibling Type ($F = 0.112$, df = 6, $p = 0.995$). A Bonferroni corrected *post hoc* analysis of these results for Sibling Type revealed that male mice raised with KO brothers had an increased level of WB activity with respect to males raised with WT brothers ($p = 0.016$).

Subsequent analysis on individual non-normalized male nuclei using a two-way ANOVA for Genotype and Sibling type with Hochberg's GT2 *post hoc* indicated that significant differences

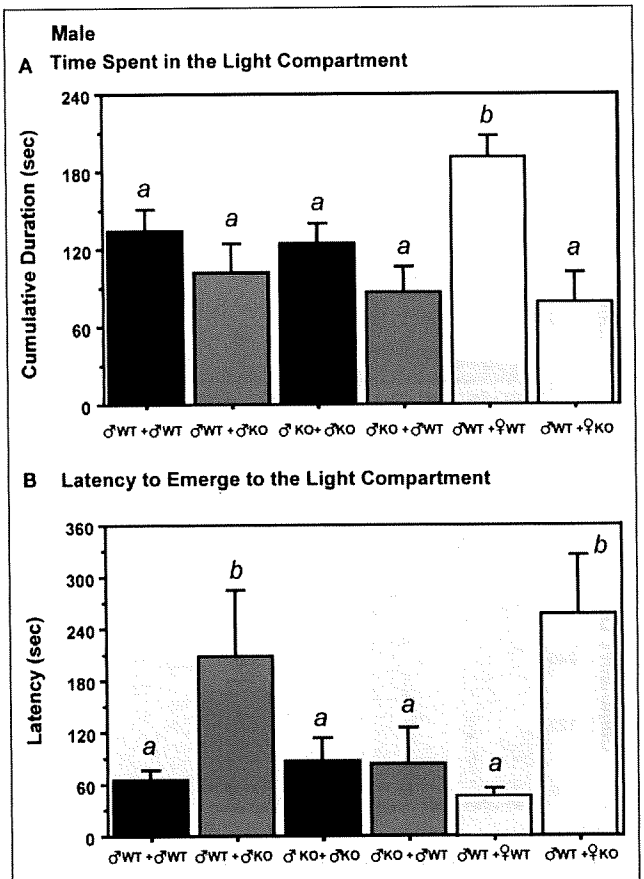

FIGURE 4 | The presence of different genotype of littermates influence later adult behavior in gonadally intact adult male estrogen receptor α knockout (ERKO) mice in Light:Dark transition tests. (A) Represents the time (s) spent in the light compartment. **(B)** Indicates the latency to emerge to the light compartment. Mean and SE is indicated; letters above bars indicate significant differences.

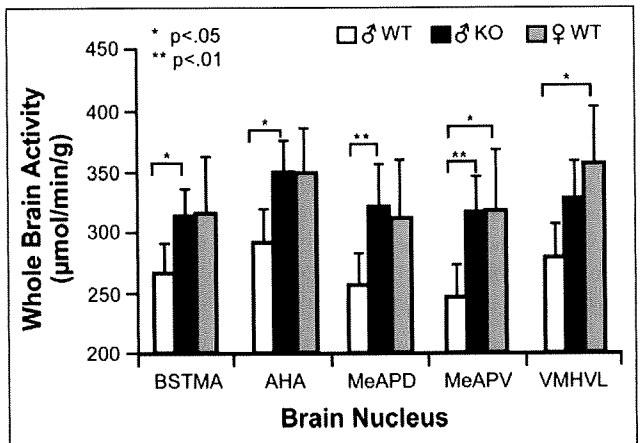

FIGURE 5 | Sibling Type affects metabolic activity in limbic nuclei of male mice in this study. Hochberg's GT2 *post hoc* analysis for a two-way ANOVA comparing sibling type and genotype effects per nucleus showed only significant sibling type effects on metabolic activity in 5 of the 20 limbic nuclei studied in the male mice. Mean and 95% confidence intervals depicted with one asterisk indicating a significance of $p < 0.05$ and two asterisks a significance of $p < 0.01$. Abbreviations: BSTMA, bed nucleus of the stria terminalis medial division, anterior; AHA, anterior hypothalamic area, anterior; MeAPD, medial amygdaloid (MeA) nucleus, posterodorsal; MeAPV, medial amygdaloid (MeA) nucleus, posteroventral; VMHVL, ventromedial hypothalamic nucleus, ventrolateral.

Table 2 | Two-way ANOVA based on the effect an individual's Genotype and Sibling Type has on cytochrome oxidase activity in whole brain measures of limbic areas in male and female mice raised in reconstituted litters.

Variable	df	*F*-value	Significance
MALES			
Genotype	1	7.435	0.518
Sibling Type	3	7.436	0.005
Genotype X Sibling type	1	0.095	0.540
FEMALES			
Genotype	1	72.319	0.000
Sibling Type	2	20.511	0.000
Genotype X Sibling type	2	2.683	0.069

were attributable only to Sibling type and not to Genotype type, conferring with the results seen in the WB analysis. In five of the 20 nuclei measured (BSTMA, AHA, MeAPD, MeAPV, and VMHVL) (**Figure 5**), males raised with WT brothers had significantly lower mean COX activity ($p < 0.05$) compared to males raised with KO brothers. For example, ♂WT raised with WT brothers had significantly lower average metabolic activity in the AHA, BSTMA, MeAPD, and MeAPV when compared to ♂WT raised with KO brothers, and lower activity in the MeAPV and VMHVL relative to ♂WT raised with WT sisters.

CYTOCHROME OXIDASE ACTIVITY: FEMALES

Analysis of female WB activity showed that both the experimental factors of Genotype and Sibling Type significantly affected the mean WB activity (**Table 2**). Comparison of the means for Genotype shows that ♀WT show a greater overall WB activity when compared to ♀KO ($p < 0.001$). A Bonferroni *post hoc* analysis showed female mice raised with ♀WT siblings had a significantly greater ($p < 0.01$) mean WB activity when compared to females raised with ♂WT or ♀KO littermates. These results for females differ from results for males as males had no significant effect of Genotype on WB, and the effect of Sibling Type on each sex appears to differ reciprocally.

A two-way ANOVA on each nucleus using the factors of Sibling Type and Genotype with Hochberg's GT2 *post hoc* analysis indicate that both Sibling Type and Genotype caused significant ($p < 0.05$) mean differences in certain nuclei activities for the females. In 10 nuclei the mean COX activity differed significantly for Genotype: cMPOA ($p = 0.013$), AHA ($p = 0.009$), PaN ($p = 0.004$), MeAA ($p = 0.005$), CeA ($p = 0.033$), VMH ($p = 0.001$), MeAPV ($p = 0.049$), VMHDM ($p = 0.027$), and VMHVL ($p = 0.004$). In each, the ♀KO had consistently lower mean nuclei activity, which agrees with the lower activity seen for the same comparison with mean WB activity in females. The analysis also showed a less extensive affect on mean nuclei activity due to Sibling Type, with significant effects found

only in the cMPOA ($p = 0.016$), AHA ($p = 0.043$), and VMHVL ($p = 0.017$).

CORRELATIONS IN CYTOCHROME OXIDASE ACTIVITY IN MALES AND FEMALES

After assessing the effects on overall mean activity of the WB and individual nuclei, interactions between the nuclei were assessed for significance. An initial analysis using Pearson's bivariate correlations on normalized nuclei measures with a two-tailed test of significance showed that males had 83 out of 190 possible pair-wise correlations significant at $p < 0.05$ and 60 out of 190 pair-wise correlations significant at $p < 0.01$ without jackknifing. Females showed 87 out of 210 possible interactions that were significant at $p < 0.05$, and 37 out of 210 at $p < 0.01$ (the increased number of possible interactions due to the inclusion of extra nuclei). When females are compared to the males, the fraction of significant interactions and number of reliably significant interactions is lower in females. This indicates that female nuclei interactions, as shown by correlated COX activity between nuclei tested, are probably not as strong as that shown in males.

PRINCIPAL COMPONENTS ANALYSIS, INTER-REGIONAL CORRELATIONS IN METABOLIC ACTIVITY, AND LIMBIC LANDSCAPES

To find functionally interactive networks, PCs were extracted for three different groups in each sex, making a total of six groups overall. These groups were all ♂(both WT and KO), all ♀ (both WT and KO), ♂WT males only, ♀WT only, ♂KO only, and ♀KO only. Finally, the Limbic Landscape method described in Crews et al. (2006) to illustrate how activity in a defined network of limbic nuclei was modified by the litter environment.

Males

Principal components analysis. Principal components for males were extracted for three different groups: all males (♂WT and ♂KO), ♂WT only, and ♂KO only. The plots of sequentially derived eigenvalues are given as SCREE plots for each group subjected to PCA, shown in **Figure 2**. Using the eigenvalues derived from PCA, the three criteria for determining significant PCs were applied to the eigenvalues of each PC in the three groups. Those eigenvalues that passed the first criterion of $l^2 > 1$ are given in **Tables 3A,B** along with the test for significance based on Eq. 1 from the second criterion; there was no case where the third criterion was invalid and all other criteria were found significant.

When both ♂WT and ♂KO were combined there were two significant PCs (significance ≥ 3.0) and when ♂WT and ♂KO males were considered separately, there was only one significant PC in each. The significant PCs in the individual ♂WT and ♂KO groups had several nuclei with coefficients greater than 0.60 (**Table 3A**) that shared coefficients of similar strength to those in the PCA of combined males. Furthermore, in the ♂WT and ♂KO groups the second, non-significant PC (included for comparison in **Table 3A**) differed from the first significant PC in its respective group for the values of its coefficients, but shared many similarities in coefficient values with the significant PC of the other male group as well as a significant PC of the combined males group. For example, the second PC for ♂WT was dissimilar to the first PC in that group, but similar to the first significant PC in ♂KO and the second significant PC in the combined males group (**Table 3A**).

After consideration, the similarity between PCs in each group of males suggests only two significant PCs that are consistent across genotype. Consequently, nuclei with a coefficient greater than 0.60 in significant PCs believed to be similar were placed together to represent one of the two putatively conserved clusters of nuclei (**Table 3B**). The first significant cluster contained several rostral amygdalar and hypothalamic nuclei. This cluster was labeled as the male rostral limbic cluster (mRLC) and contained the following nuclei: AVPe, cMPOA, AHA, PaN, VMH, MeAA, CeA, and ACo. The second cluster was labeled the male caudal limbic cluster (mCLC) and contained hypothalamic and amygdalar nuclei that were caudal to those used in the mRLC. The nuclei in the mCLC were VMH, PaN, MeAPD, MeAPV, VMHDM, and VMHVL. The inclusion of the PaN, which was not significant in any PCs of the mCLC, served as a control of between cluster correlations as the VMH showed strong correlations in both clusters. It also served as a control for demonstrating that the choice of 0.6 as the coefficient of significance was reasonable.

Inter-regional correlations in metabolic activity. Before the jackknifing procedure could be conducted, the combined male data set was subdivided into groups of shared experimental traits. These groups consisted of all animals that had the same treatment with regard to a given experimental variable. For example, ♂WT mice raised with either ♂WT or ♂KO brothers shared a similar Genotype but not Sibling Type, and were grouped together to form a ♂WT group for Genotype comparison. When the groups had been appropriately partitioned, only the nuclei within a certain cluster were used during the jackknifing procedure for that group. At the completion of jackknifing all groups had been jackknifed for both the mRLC and the mCLC (Table 1A in Supplementary Material). In many groups there were still several between nuclei correlations that maintained significance at $\alpha = 0.05$ throughout the jackknifing procedure. Further analysis also used a values of $\alpha = 0.02$ and 0.01. Within each colored cell of Table 1A in Supplementary Material is the averaged pair-wise correlation coefficient following jackknifing for the two nuclei that are denoted above and to the right of the cell. The significance of each correlation, significant and insignificant, is shown in Table 1B in Supplementary Material. Only half of each table is shown due to the symmetric nature of a pair-wise correlations table. Those correlations that were not significantly different from $r = 0$ at $\alpha = 0.05$ were deemed insignificant and were not included in Table 1B in Supplementary Material. If after jackknifing two nuclei maintain a significant correlation, then the two nuclei may be considered functionally associated, coupled, or connected. If functional connections were found between comparable groups, then a *t*-test with an assumption of unequal variance was performed on the correlation coefficients for the connection in each group. This analysis yielded several significant differences for functional connections between different Genotypes and Sibling Types.

Several nuclei showed functional associations in both ♂WT and ♂KO mice (**Figure 6**, top panel), while other functional associations were unique to ♂WT and ♂KO mice (**Figure 6**, bottom panel). Common functional associations, at $\alpha = 0.01$, were found among the amygdalar nuclei in the mRLC are: the ACo with the CeA and MeAA, and the MeAA with the CeA, PaN and VMH. In the mCLC

Table 3 | (A) Principal component analysis (PCA) of three groups of males [all males, wildtype (WT) males only, and estrogen receptor α knockout (ERKO) males only]. For each group there were 20 principal components (PCs), but only those given below satisfied the first criterion of $I^2 > 1$. Significant eigenvalues, marked as bolded numbers with asterisks, satisfied the second and third criterion. Other eigenvalues that shared similarities to significant eigenvalues in other groups are marked with a tilde (~). Both marked eigenvalues correspond to PCs that were considered in later analyses. **(B)** Rotated component matrix with significant PCs derived from the principal component analysis displayed in **Table 3A**. The columns are the significant PCs and PCs of shared similarity to significant PCs in other groups. The coefficient value for each PC is given after VARIMAX rotation.

	All ♂			♂WT only			♂ERKO only		
	Eigenvalue	**% Variance**	**Sign.**	**Eigenvalue**	**% Variance**	**Sign.**	**Eigenvalue**	**% Variance**	**Sign.**
A. PRINCIPAL COMPONENT ANALYSIS									
1	7.687	38.436	***8.247**	7.363	36.814	***4.306**	8.638	43.192	***5.973**
2	2.582	12.910	***3.729**	3.165	15.827	~2.196	3.340	16.698	~1.358
3	1.963	9.817	0.359	2.190	10.951	0.807	2.453	12.266	1.355
4	1.797	8.985	1.715	1.746	8.728	2.381	1.800	9.000	0.828
5	1.334	6.670	0.787	1.196	5.978	0.239	1.318	6.590	0.791
6	1.064	5.321	0.476						

	All ♂		♂WT only		♂ERKO only	
	***1**	***2**	***1**	**2**	***1**	**2**
B. MATRIX COMPONENT						
rMPOA	0.04	−0.05	0.22	0.01	0.11	−0.18
BST	−0.07	0.07	−0.05	−0.10	0.06	−0.05
BSTMA	0.40	0.25	0.13	0.25	0.29	0.45
AVPe	0.52	−0.15	***0.70**	0.04	−0.13	0.52
Pe	0.15	0.06	0.41	0.09	0.20	0.06
MPOA	0.19	0.21	0.41	0.36	0.23	0.11
BSTMPM	0.08	−0.07	0.01	−0.26	0.12	0.07
cMPOA	0.53	0.31	***0.67**	0.44	0.35	0.43
ACo	***0.84**	0.25	***0.92**	0.07	0.57	0.66
AHA	***0.78**	0.14	***0.69**	0.22	0.21	0.87
PaN	***0.84**	0.19	***0.66**	0.47	0.14	0.95
CeA	***0.84**	0.19	***0.89**	0.04	0.45	0.71
MeAA	***0.84**	0.22	***0.84**	0.04	0.46	0.73
MHb	0.25	0.00	0.36	0.07	0.05	0.20
LHb	−0.13	0.06	−0.05	0.14	−0.05	−0.23
VMH	0.56	0.45	***0.65**	0.28	***0.78**	0.36
MeAPD	0.38	***0.81**	0.15	0.71	***0.84**	0.35
MeAPV	0.26	***0.90**	−0.05	0.90	***0.86**	0.36
VMHDM	0.22	***0.80**	0.28	0.83	***0.87**	0.12
VMHDL	0.09	***0.86**	0.12	0.90	***0.90**	0.05

Asterisk indicates nuclei with a coefficient greater than 0.60 in significant PCs. These significant nuclei were placed in a cluster of nuclei representative of one of the two putatively conserved PCs. These probable conserved clusters can be noted by comparing coefficient values between PCs thought to conform to the same cluster such as PC 1 in all ♂ mice, PC 1 in ♂WT only, and PC 2 in ♂KO only. Significant values and PCs are indicated by bold numbers with asterisks.

common associations were between proximal subnuclei – the MeAPD with the MeAPV and the VMHVL with the VMHDM. It should be noted that there were no significant associations between these two clusters that are shared across genotypes.

Given the large number of functional associations shared by either genotype, there were still many functional associations that were unique to ♂WT mice. In the mRLC these include associations by the AHA with the cMPOA, CeA, PaN, VMH, and MeAA; by the VMH with the PaN, AVPe; and by the CeA with the cMPOA. In the mCLC of the ♂WT mice, unique functional associations are limited to the MeAPV with the VMHDM and VMHVL. In the ♂KO mice there are fewer functional associations: in the mRLC these are made by the cMPOA with the VMH and the MeAA and by the CeA with the PaN. In the mCLC, ♂KO mice had a functional association of the VMH with the MeAPD and the MeAPV.

Similarly, there were common functional associations among males that are housed with either ♂WT or ♂KO brothers (**Figure 7**, top panel), but other functional associations that were unique to males raised with ♂WT or ♂KO brothers (**Figure 7**, bottom panel).

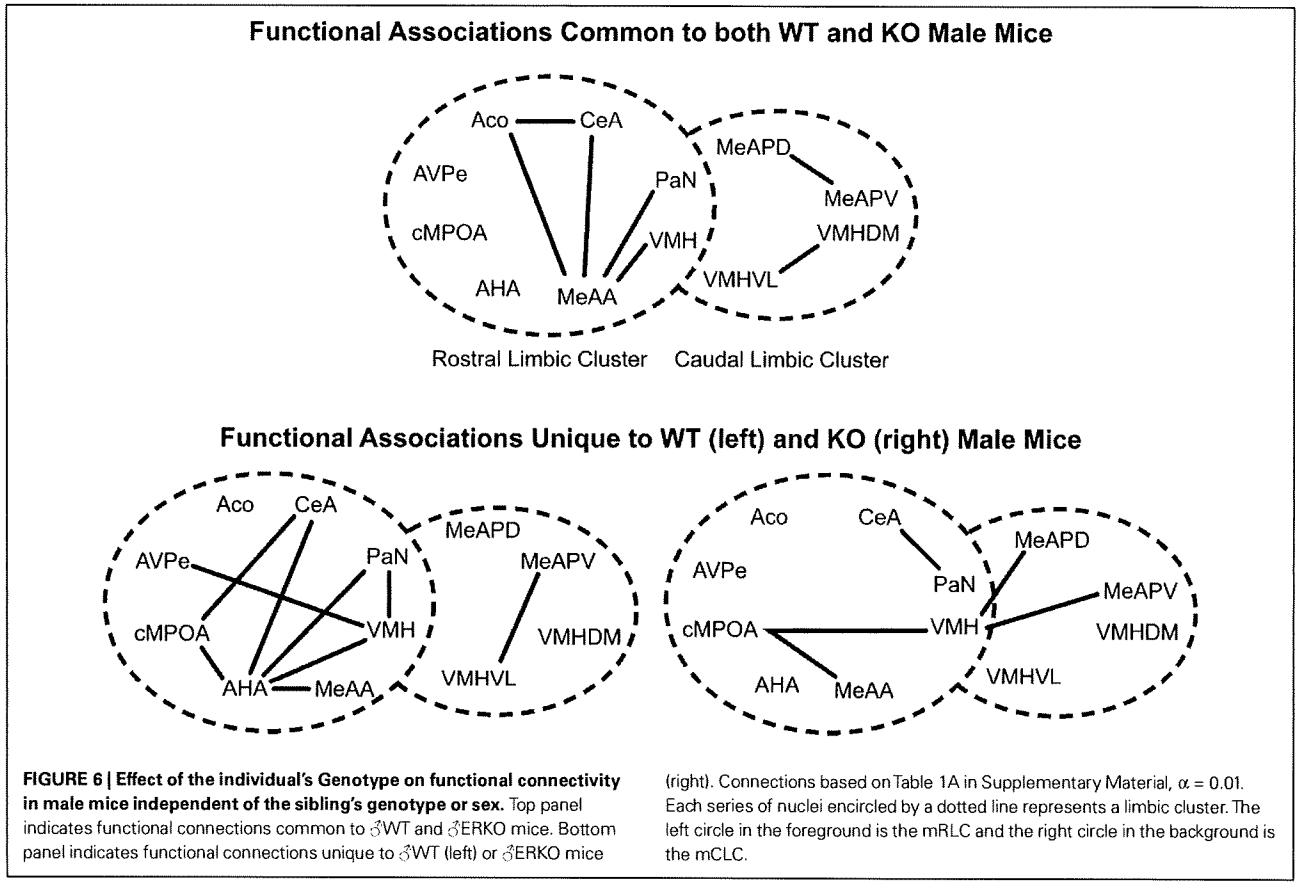

FIGURE 6 | Effect of the individual's Genotype on functional connectivity in male mice independent of the sibling's genotype or sex. Top panel indicates functional connections common to ♂WT and ♂ERKO mice. Bottom panel indicates functional connections unique to ♂WT (left) or ♂ERKO mice (right). Connections based on Table 1A in Supplementary Material, $\alpha = 0.01$. Each series of nuclei encircled by a dotted line represents a limbic cluster. The left circle in the foreground is the mRLC and the right circle in the background is the mCLC.

Common associations were found among the amygdalar nuclei: the ACo with CeA, the CeA with MeAA, and the MeAA with the VMH in the mRLC. Functional associations also occurred between the MeAPD and MeAPV and between the VMHDM and VMHVL in the mCLC. Again, there were no significant associations between nuclei of the mRLC and mCLC suite of nuclei shared between Sibling Type groups. As with the male mice in this study, having a WT brother resulted in a number of unique functional associations, including significant associations between nuclei in the mRLC and mCLC suite of nuclei (**Figure 7**, top panel). These included associations of the PaN with the CeA, AHA, and VMH; the AHA with the VMH and cMPOA; and the cMPOA with the VMH in the mRLC. In the mCLC, the MeAPV associated with the PaN, VMH, and VMHVL. There were only two functional associations unique to males having KO brothers, and these were between the ACo and the MeAA in the mRLC and between the MeAPV and the VMHVL in the mCLC. The paucity of interactions for males raised with ♂KO may be due to the small sample size.

Limbic landscapes. To illustrate changes in the metabolic activity in selected nuclei (BNSTma; AVPe; MPOA; AHA; MeAPD; MeAPV; VMHVL) with defined neural connections, it is clear that the effect of having KO brothers or sisters in the litter have different consequences on WT males (**Figure 8**, bottom row). Further, in the mixed-sex, mixed-genotype litters, the effect of the genotype of the brothers or sisters had different effects on the limbic landscape of WT males (**Figure 8**, right column). The effect of Genotype in all-male litters indicated an overall decrease in activity, but no differences in activity pattern among the nuclei (**Figure 9**).

Females

Principal components analysis. In order to further compare the functional connectivity between males and females PCA was performed as before on three different groups generated from a subset of the female study population. Because of a large number of missing nuclei measures for individual animals, the full set of animals and nuclei had to be parsed to avoid the problem of missing values when performing PCA. The data set was then optimized for the maximum number of animals and nuclei. The best result featured 34 animals and 13 nuclei. Those nuclei were the LSI, MPOA, Pe, ACo, MeAA, CeAA, VMH, LHb, MHb, MeAPD, MeAPV, VMHDM, and VMHVL. It should be noted that the number of female animals used for PCA is nearly the same size as that used in the PCA of males, but with seven fewer nuclei considered. The types of groups used for PCA were discussed above.

The results of PCA for the three female groups can be visualized using the SCREE plots (**Figure 2**), and the analysis for significant PCs (**Tables 4A,B**). The number of significant PCs between groups and significant nuclei in each of those PCs are dissimilar to the results found in males. When all females were considered in the

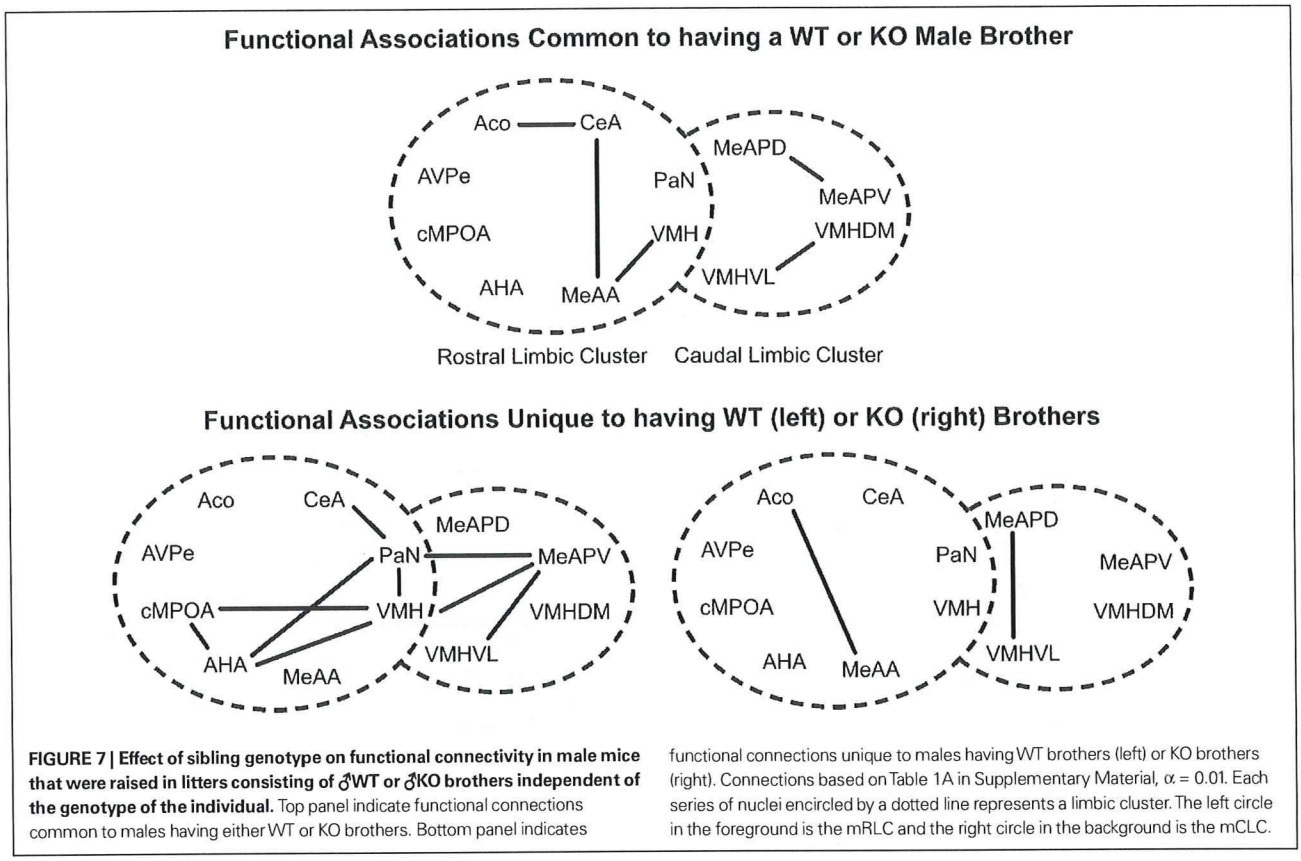

FIGURE 7 | Effect of sibling genotype on functional connectivity in male mice that were raised in litters consisting of ♂WT or ♂KO brothers independent of the genotype of the individual. Top panel indicate functional connections common to males having either WT or KO brothers. Bottom panel indicates functional connections unique to males having WT brothers (left) or KO brothers (right). Connections based on Table 1A in Supplementary Material, $\alpha = 0.01$. Each series of nuclei encircled by a dotted line represents a limbic cluster. The left circle in the foreground is the mRLC and the right circle in the background is the mCLC.

PCA there was only one significant PC, and the nuclei that showed significance were all amygdalar: ACo, MeAA, CeA, MeAPD, MeAPV. Although the subdivided groups of ♀WT and ♀KO females were evenly numbered at 17, PCA performed on each group resulted in PCs with significant nuclei that were not represented in both genotypes. The significant PCs and the significant nuclei within each of those PCs for all three groups (**Table 4A**) indicated one significant PC for all females, four significant PCs for ♀WT, and three significant PCs for ♀KO females (**Figures 10 and 11**).

These results differ from males due to two reasons: (i) There was a significant PC (PC2) in WT females with no analog in ♀KO females. (ii) Unlike males, where almost all significant nuclei in similar PCs were at or near significance between genotypes, similar PCs in females only contained a majority of shared significant nuclei between genotypes. Also, when comparing similar PCs between genotypes many nuclei showing significance in one genotype were not even near significance in the other.

Inter-regional correlations in metabolic activity. Although these significant clusters were less conserved than in the males, a jackknifing analysis was still conducted by genotype to distinguish the nature of the connectivity between different genotypes and to indicate qualitatively the difference between sexes. From the three possible similar PCs, only two showed an indication of multinuclei connections or clusters (>2 shared nuclei, with a majority of the nuclei in each PC shared) among female mice (**Table 4B**). These clusters shared some similarities to males in the nuclei considered, but were otherwise quite distinct (**Figures 10 and 11**). The more rostral of the two clusters, the female rostral limbic cluster contained the Pe, ACo, MeAA, CeA, MeAPD, and MeAPV, while the more caudal cluster, female caudal limbic cluster contained the LHb, MeAPV, VMH, VMHDM, and VMHVL. Like the males, the females maintained a cluster of nuclei associated with the amygdala and a cluster associated with the VMH and subnuclei, however this appeared to be the extent of the similarity. As before, nuclei were selected to enter into the cluster if significance was shown in either of the putative clusters. Results of the jackknifing can be seen in **Table 4B** for a comparison of genotype, and further demonstrated the differing nature of male and female connectivity.

Limbic landscapes. Mapping the limbic landscape in selected nuclei with defined neural connections, it is clear that the effect of having KO brothers or sisters in the litter have different consequences on WT females (**Figure 12**, bottom row). Further, in the mixed-sex, mixed-genotype litters, the effect of the genotype of the brothers or sisters had different effects on the limbic landscape of WT males (**Figure 8**, right column). The effect of Genotype in all male litters indicted an overall decrease in activity, but no differences in the pattern of activity among the nuclei (**Figure 9**).

DISCUSSION

An individual's genotype interacts with its environment throughout life to continuously shape the phenotype. In mammals, the formative environment for social and anxiety-related behaviors

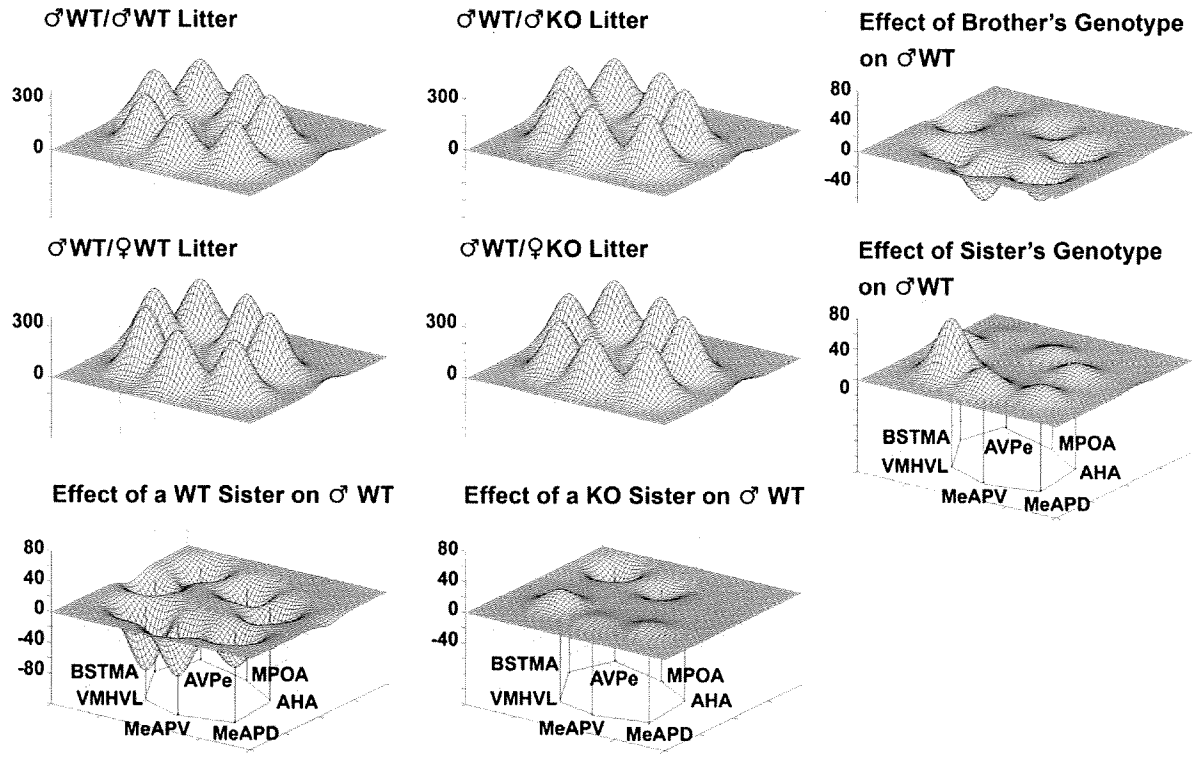

FIGURE 8 | The Sex and Genotype of siblings in the litter influences metabolic activity in the limbic landscape of adult male mice wildtype (WT) for the estrogen receptor a gene. Limbic landscapes of ♂WT raised with brothers or sisters of the same or different genotype are depicted. Illustrated is the mean cytochrome oxidase (COX) activity in each nucleus of each ♂WT. Groups are presented according to the type of sibling with which the ♂WT individual was raised; ♂WT; ♂KO; ♀WT; ♀KO. The limbic landscape maps on the bottom row give the difference between the ♂WT/♂WT and ♂WT/♀WT (left) and the ♂WT/♂WT and ♂WT/♀KO maps (right), indicating the effect of the sister's genotype on ♂WT. The far right column indicates the effect of sibling's genotype; on the right top is the effect of the brother's genotype and in the middle row is the effect of sister's genotype; the far right column is the difference between the ♂WT/♂WT and ♂WT/♂KO (top right) and the ♂WT/♀WT and ♂WT/♀KO maps (middle right). The nuclei are presented in a clockwise fashion reflecting a rostral-caudal dimension: main bed nucleus of the stria terminalis (BNSTma); anteroventral periventricular nucleus (AVPe); medial preoptic area (MPOA); anterior hypothalamus, anterior (AHA); medial amygdaloid nucleus, posterodorsal (MeAPD); medial amygdaloid nucleus, posteroventral (MeAPV); ventromedial hypothalamic nucleus, ventrolateral (VMHVL).

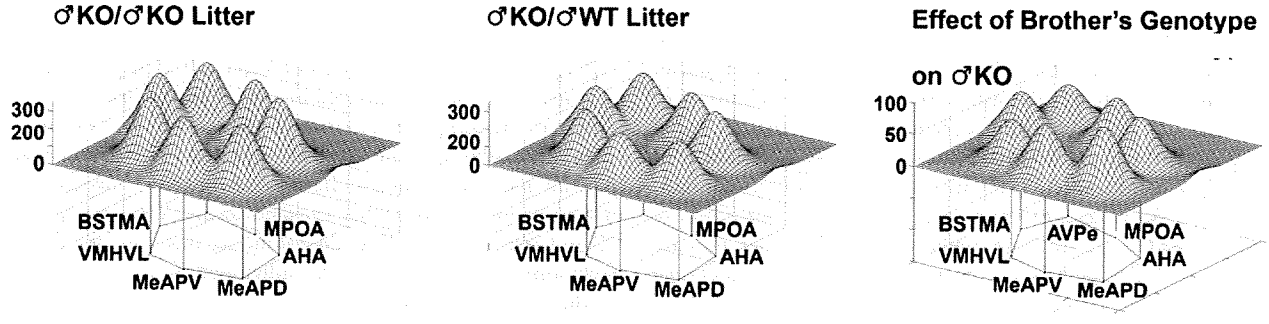

FIGURE 9 | The genotype of brothers in the litter influences metabolic activity in the limbic landscape of adult male estrogen receptor α knockout mice (♂KO). Groups presented according to the type of sibling with which the male was raised (with ♂KO or ♂WT brothers). The limbic landscape map on the right represents the difference between ♂KO/♂KO litter and ♂KO/♂WT litter, or the Effect of the Brother's Genotype on ♂KO mice. Other details as in **Figure 8**.

is the family unit; in the case of rodents, this is the litter and the mother-young bond. A deciding factor in this environment is the sex ratio of the litter and, in the case of mice lacking functional copies of gene(s), the ratio of the various genotypes in the litter. A summary of the behavioral data obtained with males indicate that when raised in litters having either ♂KO or ♀KO littermates, ♂WT are more aggressive than when raised in litters containing either ♂WT or ♀WT littermates. KO males are not aggressive